July 14, 2022

Inositol phosphorlyceramide synthase null *Leishmania major* are viable and virulent in animal infections where salvage of host sphingomyelin predominates

F. Matthew Kuhlmann[1,2], Phillip N. Key[1], Suzanne M. Hickerson[1], John Turk[2, $], Fong-Fu Hsu[2], and Stephen M. Beverley[1,*]

[1] Department of Molecular Microbiology, and [2] Department of Internal Medicine, Washington University School of Medicine, 660 S. Euclid Ave., Saint Louis, MO 63110, USA. [$] Deceased.

*Corresponding author: Stephen M. Beverley, Department of Molecular Microbiology, Box 8230, Washington University School of Medicine, 660 S. Euclid Ave., Saint Louis, MO 63110, USA. Tel: 314-747-2630, Fax: 314-747-2634; E-mail: stephen.beverley@wustl.edu

Keywords: Trypanosomatid protozoan parasite; Sphingolipids, inositol phorphorylceramide, lipid remodeling, lipid salvage, infectivity and virulence.

Running Title: Virulent *Leishmania* IPCS knockouts survive by sphingomyelin salvage

Abstract

Many pathogens synthesize inositolphosphorylceramide (IPC) as the major sphingolipid (SL), differing from the mammalian host where sphingomyelin or more complex SLs predominate. Thus, divergence between IPCS and mammalian sphingolipid synthases has prompted interest as a potential drug target. However, in the trypanosomatid protozoan *Leishmania*, promastigotes lacking *de novo* sphingolipid synthesis (Δ*spt2-*) survive and remain virulent, as amastigotes salvage host sphingolipids and are still able to produce IPC. To further understand the role of IPC, we generated null IPCS mutants in *L. major* (Δ*ipcs*$^-$). Unexpectedly and unlike fungi where IPCS is essential, Δ*ipcs*$^-$ was remarkably normal in culture and highly virulent in mouse infections. Both IPCS activity and IPC were absent in Δ*ipcs*$^-$ promastigotes and amastigotes, arguing against an alternative route of IPC synthesis. Notably, salvaged mammalian sphingomyelin (SM) was highly abundant in purified amastigotes from both WT and Δ*ipcs*$^-$. Quantitative estimation showed SM to be about 7-fold more abundant than IPC in WT amastigotes, suggesting that normally, SM is the dominant amastigote SL. These data suggest that SM salvage may account for the survival and virulence of Δ*ipcs*$^-$, a finding with some implication towards the suitability of IPCS as a chemotherapeutic target.

Introduction

Leishmaniasis is often considered a neglected tropical disease. Currently it is estimated that there are more than 1.7 billion people at risk and nearly 12 million people with symptomatic disease, ranging from mild cutaneous infections to severe disfiguring or lethal forms, with upwards of 50,000 deaths annually (1-4). Remarkably, the great majority of infections are undiagnosed and/or asymptomatic, suggesting that well more than 100 million people may harbor parasites (3,5). Persistent asymptomatic infections constitute a double edged sword – while serving as a reservoir for transmission and/or reactivation by stress or immunosuppression, persistent parasites are known to mediate strong protective concomitant immunity against disease pathology (3,5-7). *Leishmania* have two distinct growth stages, a promastigote stage in the sand fly vector, and an intracellular amastigote stage residing within cellular endocytic pathways in the mammalian host (4). While the promastigote stage is readily cultured in the laboratory and amenable to molecular techniques, amastigotes require the use of macrophage infection systems or infections of animal models replicating key aspects of human disease.

While progress has been achieved in new chemotherapeutic strategies, many are not yet implemented clinically and resistance to several promising agents has already been observed (8-10). One pathway potentially offering important drug target is that of sphingolipid synthesis (11-13). Sphingolipids (SL) are a diverse class of lipids that function in apoptosis, cell signaling, and membrane structure and these pathways have been targeted for therapies against a wide range of diseases including cancer, multiple sclerosis, and infectious diseases (14-18). Sphingolipids differ in the nature of the head groups as well as the composition of the hydrophobic ceramide anchor, in different tissues and species. Unlike mammalian cells that primarily synthesize sphingomyelin (SM) and complex glycosphingolipids, *Leishmania* synthesize inositol

phosphorylceramide (IPC) as their primary sphingolipid (19), as do other protozoa, fungi and plants (11,20,21).

This divergence has prompted scrutiny of IPCS as a drug target, where in fungi it is essential and repression causes decreased growth and virulence along with increased susceptibility to acidic environments (22,23). IPC is formed when inositol phosphorylceramide synthase (IPCS) converts ceramide and phophatidylinositol (PI) to IPC and diacylglycerol (DAG). The related trypanosomatid parasite *Trypanosoma brucei* encodes four sphingolipid synthases (SLS), collectively mediating synthesis of sphingomyelin (SM), ethanolamine phosphorylceramide and IPC; inducible RNAi knockdowns of the entire locus were lethal, although the contribution of the individual genes/activities was not further dissected (24). *Leishmania* IPCS has been pursued as a drug target by analogy of findings from pathogenic fungi as well as its divergence from mammalian sphingomyelin synthases (25). While aureobasidin A, a known inhibitor of yeast IPCS, was inactive against *Leishmania* and *Trypanasoma cruzi* (26), other studies have revealed candidate inhibitors (26-30).

Notably, the biological requirement for *Leishmania* IPCS has not been addressed *in vivo*. That *Leishmania* could differ from other organisms was first suggested by the fact that *L. major* null mutants lacking the first enzyme in *de novo* sphingolipid synthesis, serine palmitoyl transferase (Δ*spt2*$^-$) completely lacked all SLs, yet remain viable in log phase culture (31,32). Subsequent studies in promastigotes showed that sphingolipid catabolism was used to generate ethanolamine (EtN), whose provision to Δ*spt2*$^-$ parasites rescued a defect in differentiation to infective metacyclic parasites (33). While Δ*spt2*$^-$ was fully infective in animal models, it continued to synthesize IPC, presumably by salvage of potential precursor sphingolipid components from the host cell (34-36). Several routes could be envisaged; sphingoid (long-

chain) bases or ceramide precursors could be salvaged directly, or mammalian sphingolipids could be acquired and catabolized for resynthesis as IPC sphingolipids. As all routes ultimately require IPCS for parasite IPC synthesis, we sought to generate Δ*ipcs*⁻ null mutants if possible, and to explore their impact on IPC synthesis and/or metabolism, and virulence in animal models. Surprisingly, our data show convincingly *IPCS* was not essential, with SM salvage in WT cells rendering it the dominant amastigote SL as well as serving as the source of amastigote IPC. These findings account for the dispensability of IPCS in animal infections, potentially dampening enthusiasm for IPCS as a useful drug target in this parasite.

Results

Targeted Replacement of *L. major IPCS*. The *L. major* genome is primarily diploid albeit with occasional aneuploidy, and typically two rounds of gene replacement are required to generate null mutants of single copy genes (37). Targeting constructs containing resistance markers to G418 (*NEO)* or nourseothricin (*SAT*) were designed to successively replace the *IPCS* ORF precisely by homologous gene replacement (Fig. 1A). To alleviate concerns about lethality of IPCS deficiency, we focused on the culturable promastigote stage where SLs are not required in any capacity in the presence of ethanolamine (31-33). A secondary effect of IPCS deficiency could be ceramide accumulation which can be toxic (38), and we also performed transfections in the presence of myriocin (an inhibitor of *de novo* SL synthesis) to potentially ameliorate this.

Heterozygous (*IPCS/IPCS::ΔNEO*) and homozygous null mutants (*IPCS*::Δ*SAT*/*IPCS*::Δ*NEO*; referred to as *Δipcs*⁻) were readily obtained and confirmed by PCR tests to lack the IPCS coding region, accompanied by the expected planned replacements (analysis of the double homozygous replacement is shown in Fig. 1B). An episomal expression vector (pXG-BSD-IPCS) was used to restore *IPCS* expression, yielding the line *Δipcs*⁻/+*IPCS*

(Fig. 1 A,B). The recovery of *Δipcs*⁻ clonal lines was readily accomplished with good efficiencies, regardless of EtN or myriocin treatment, and these showed no obvious growth defects. Numerous transfectant lines were obtained and authenticated with similar phenotypes, and in this work results from one representative set of KO and IPCS-restored pair are shown.

IPCS activity is lost in *Δipcs*⁻ promastigotes. Enzymatic assays with promastigote microsomes were performed by evaluating the conversion of phosphatidylinositol (PI) and NBD-Ceramide to NBD-IPC, after TLC separation, and quantitative fluoroscopy (Figs. 2A, S1A). High levels of NBD-IPC were generated in complete reactions bearing microsomes, NBD-Cer and PI; this product was sensitive to PI-PLC digestion as expected. We purified and confirmed the presumptive NBD-IPC from the TLC plate by mass spectrometry[1]. Consistent with prior studies, aureobasidin A did not inhibit the *in vitro* reaction (26). Little or no product was obtained if PI or NBD-Cer were omitted, if PC replaced PI, or if microsomes were omitted or previously heat inactivated. These data confirmed our ability to assay IPCS, with the expected enzymatic properties (Figs. 2A, S2A).

We compared the IPCS activity of WT, *Δipcs*⁻/+ or *Δipcs*⁻/+ *IPCS* parasite microsomes (Figs. 2B, S1B). As expected, *Δipcs*⁻ showed no detectable activity, while *Δipcs*⁻/+ IPCS showed about 50% more than WT.

***Δipcs*⁻ promastigotes lack IPC.** Mass spectrometry was used to evaluate lipids present in whole cell extracts of WT, *Δipcs*⁻ and *Δipcs*⁻*/+IPCS* promastigotes (Fig. 3A-C). In WT, two ion peaks at *m/z* 778.6 and 806.6 corresponding to $[M – H]^-$ ions of d16:1/18:0- and d18:1/18:0–IPC respectively were seen, as described previously (32,34,39). Consistent with the genetic deletion

[1] Data not shown.

of IPCS, these IPC ions were undetectable in *Δipcs*⁻ promastigotes. IPC levels were restored in the *Δipcs*⁻/+*IPCS* promastigotes, albeit only partially to about 50% WT levels (Fig. 3C).

Together with the results from enzymatic assays, these data established that *Leishmania* IPCS is the sole source of IPCS enzymatic activity or IPC.

As predicted, IPC precursor d16:1/18:0-ceramide (*m/z* 536.6) levels were elevated in the *Δipcs*⁻ promastigotes (Fig. 3B) relative to WT cells (Fig 3A). Curiously, this ceramide peak did not decrease noticeably in *Δipcs*⁻/+*IPCS*, despite restoration of IPC levels (Fig. 3C). Small variations in the levels of PE ions of *m/z* 726.6 (*p*18:0/18:2-PE) and 728.6 (*p*18:0/18:1-PE) were seen, but the levels of other lipids identified by MS such as ions at *m/z* 849 (e18:0/18:1-PI) and 863 (18:0/18:1-PI), did not appear to change in either *Δipcs*⁻ or *Δipcs*⁻/+*IPCS* promastigotes (Fig. 3A-3C). The causes of these minor changes were not pursued further.

***Δipcs*⁻ promastigotes remain viable and form metacyclics.** As promastigotes *in vitro*, *Δipcs*⁻ grew somewhat slower than WT, with a doubling time of 9.0 ± 0.7 hours vs. 7.7 ± 0.4 (mean ± 1SD, n=3) hours for WT, reaching a stationary phase density of about 70% WT (Fig. 4A). Upon entry into stationary phase a small percentage of nonviable cells emerged, as judged by propidium iodide exclusion (Fig. 4B). Since *Δipcs*⁻ promastigotes should retain sphingolipids capable of generating EtN (33), we suspected that provision of EtN would have no effect on stationary phase viability, which proved correct (Fig. S2 A,B). Restoration of IPCS expression in the *Δipcs*⁻/+*IPCS* line returned growth and viability to WT (Fig. 4A,B).

Upon entry into stationary phase *Leishmania* promastigotes differentiate to an infective metacyclic form that can be purified by lectin or density-gradient methods (40). *Δipcs*⁻ showed a

small reduction in metacyclics relative to WT or the *Δipcs*⁻/+*IPCS* control (7.5 ± 5.3% in *Δipcs*⁻ vs. 12.5 ± 8.5% in WT, or 10.7 ± 4.6%, *Δipcs*⁻/+*IPCS*; n = 2; Fig. S2C).

***Δipcs*⁻ promastigotes are hyper-susceptible to exogenous sphingoid bases.** Accumulation of ceramide, SBs, or their phosphorylated forms is toxic to most eukaryotic cells (38). This suggested that in the absence of further metabolism by IPCS, addition of exogenous SBs would likely lead to excess toxic ceramide or SB levels in *Δipcs*⁻. Accordingly, daily addition of 2 μM 3-keto-dihydrosphingosine, dihydrosphingosine, or C17 phytosphingosine resulted in death of *Δipcs*⁻ parasites (KDS shown in Fig. 4C; others not shown), which was rescued in *Δipcs*⁻/+*IPCS*. For cultures receiving C17 phytosphingosine, mass spectrometry confirmed synthesis of phytoceramide (Fig. S3).

***Leishmania Δipcs*⁻ promastigotes are susceptible to extreme pH but not temperature stress.** *IPCS* null *Cryptococcus neoformans* is susceptible to pH but not temperature stress (22), and we obtained similar results for *L. major Δipcs*⁻ promastigotes. At pH 4.0 all cells died, while at pH 5.0, *Δipcs*⁻ grew much slower (Fig. 4D), but at pH 5.5 and above minimal differences were seen (Supplemental Table S2). Temperature stress was tested at 30º and 33º C with minimal effect on relative *Δipcs*⁻ growth (Fig. S2D); at 37º C, all cells died.

***Δipcs*⁻ defects are not reversed by diacylglycerol.** The IPCS product DAG also functions as a messenger in multiple signaling pathways mediated by Protein Kinase C (PKC). *Leishmania* lack a known PKC although it has been suggested that other kinases may fulfill similar roles (41). We tested the ability of exogenous DAG to rescue the growth or viability reductions seen in *Δipcs*⁻ promastigotes by adding DAG daily to cultures. However, with two separate

supplementations (0.2 or 2 μM) no improvement was observed (Figs. S2E,F), suggesting that DAG deficiency did not contribute to *Δipcs*$^-$ phenotypes.

***Δipcs*$^-$ promastigotes are rounded but lipid bodies and acidocalcisomes are unchanged.** In Δ*spt2*$^-$ promastigotes, sphingolipid deficiency causes changes in cell rounding, acidocalcisomes, and lipid bodies (33,34). A modest effect on cell rounding was observed in *Δipcs*$^-$ (22% vs. 6% for WT or 11% for *Δipcs*$^{-/}$*+IPCS*). WT and *Δipcs*$^-$ appeared similar by DAPI staining of acidocalcisomes/polyphosphates or lipids (Nile Red O staining), and *Δipcs*$^-$ acidocalcisomes appeared structurally intact as evidenced by staining with VP1 antibody (42).

***Δipcs*$^-$ remain fully virulent in mouse infections**. To test the key question of whether *IPCS* is essential for virulence, we infected susceptible BALB/c or γ-interferon knockout C57BL/6 mice with 1 x 10^5 metacyclic promastigotes. Unexpectedly the *Δipcs*$^-$ infections progressed significantly faster than those of WT or *Δipcs*$^-$*/+IPC,* which were similar (a representative experiment is shown in Fig. 5 and combined data from four experiments is shown in Fig. S4A). Limiting dilution assays at key time points showed that regardless of genotype, lesions of similar sizes had similar parasite numbers (Fig. S4B), establishing that increased lesion size reflected increased parasite numbers primarily. These data show that if anything, *Δipcs*$^-$ was unexpectedly somewhat hypervirulent.

***Δipcs*$^-$ amastigotes lack IPC.** To eliminate the possibility that amastigotes elaborated an alternative IPCS activity, parasites were inoculated into susceptible mice, and purified from similarly sized lesions after 1-2 months. Lipids were then extracted for analysis by electrospray ionization mass spectrometry (ESI/MS) in the negative ion mode. High amounts of background signal complicated interpretations of full scan spectra (Fig. S5), which was overcome by

employing linked scan spectra using precursor ion scan of *m/z* 241 specific for detection of [M – H]$^-$ ions of PI and IPC lipids (39,43). These scans showed abundant IPC species (ions of *m/z* 778.6, 806.6 and 808.6) in purified WT amastigotes, as seen previously (Figs. 6A, S6A,G) (34), but did not reveal IPC in *Δipcs*$^-$ amastigotes, in four separate purified preparations (Figs. 6B, S6C,E,H,I). The abundance of other lipid species did not appear to change consistently or significantly (Figs. S5, S6). No significant differences were seen in amastigotes purified from BALB/c or γ-IFN knockout (γKO) C57BL/6 mice (Fig. S6H,I vs. 6A). Thus, the ability of *Δipcs*$^-$ *L. major* amastigotes to survive and induce pathology does not depend on IPC.

WT amastigotes contain abundant amounts of host derived SM. Previous studies showed that *L. major* Δ*spt2*$^-$ parasites lacking the key enzyme for *de novo* SB base synthesis nonetheless showed high levels of IPC within infected animals, suggesting that *Leishmania* amastigotes have the ability to salvage host sphingolipids (34,44). We examined this more directly by MS in purified amastigotes from both WT and *Δipcs*$^-$ parasites, which revealed high levels of ions corresponding to SM (Figs. 7A,B, S7A,G and S7C,E,H,I). While in many mammalian tissues the most abundant form of SM is d18:1/18:0 (45), in our preparations the most abundant SM was d18:1/16:0 (Figs. 7, S7). This agrees with earlier findings that d18:1/16:0-SM is the most abundant in macrophage preparations commonly used in the study of *Leishmania*, including thioglycolate-elicited peritoneal, bone marrow derived or RAW.264.7 macrophages (46,47) (Table S3). SM quantitation was achieved by measuring the ratio of the peak height of the [M + Na]$^+$ ion of d18:1/16:0-SM (*m/z* 725.7) to that of a spike-in control d18:1/12:0-SM (*m/z* 665.9) (Fig. 7A-C). The data showed that SM in WT infected mouse tissue was found to be about 1.3 times that of the purified *Δipcs*$^-$ amastigotes from two preparations.

These data suggested that the levels of salvaged mammalian SM were remarkably high in purified amastigotes. However, purified amastigotes typically are contaminated by host material, which can be readily visualized in lipid extracts from total infected footpad lesions where the mouse tissue contributions dominate (Fig. 7C). We preferred this control instead of uninfected mouse footpads, which lack the extensive infiltration of immune cell types with differing lipid profiles within infected lesions. We sought an estimate of the degree of host contamination of our purified amastigotes, a goal challenged by the complexity of the samples and mix of overlapping and unique lipids between *Leishmania* and mouse. Qualitatively, the host contamination was relatively minor, as it can be seen by the relative decrease of diverse PC species in purified amastigotes vs the whole WT infected tissue (Fig 7A,B vs 7C). Quantitatively, we estimated a relative loss of mouse lipids ranging of 16-fold for phosphatidyl cholines (range 9-26 depending on specific PC species) or 4-fold for plasmenyl cholines (range 2.6-4.8 fold depending on specific ions), consistent with the 9-fold decreased levels of IPC seen in infected tissues relative to purified amastigotes (Fig. 6A,C; calculated relative to the prominent 18:0/20:4-PI peak at *m/z* 885.8). Notwithstanding some caution that the ion (*m/z* 885) is a suitable internal control, the data clearly suggest that most of the salvaged SM in purified amastigote preparations must come from the parasite itself.

Salvaged SM and not IPC is the predominant SL in amastigotes. To corroborate the findings above, we evaluated the relative amounts of IPC and SM in WT amastigotes, where IPC is quite abundant (34). We employed a spike-in approach where non-indigenous standards expected to have similar MS ionization behavior were added to each sample, titrating the amounts in pilot studies until a similar peak height was obtained with the biological species of interest (34). The amastigote preparations were spiked with 10 nmol N-Lauryl SM and 2 nmol of dipalmitoyl PI,

followed by positive or negative ion ESI/MS (Fig. 8). For IPC, the amastigote IPC species peak heights sum to about 90% of that of the PI standard, while the amastigote SM peak height was about 130% of the SM standard (Fig. 8), suggesting the relative amounts of IPC:SM was 1:7 in the purified amastigotes. As noted earlier, only small changes in this value could be attributed to host contamination, and thus,, SM is likely the dominant sphingolipid in WT amastigotes involving in the IPC synthesis. While this assay could not be applied to *Δipcs*$^-$ amastigotes, the similar levels of SM in these relative to WT SM must likewise dominate in the mutant (Figs. 7A,B; S7A,I vs. C,E,H,I),

WT amastigotes contain IPC with mammalian-like ceramide anchors. The two promastigote IPC ions at *m/z* 778.6 and 806.6 have d16:1/18:0- and d18:1/18:0-Cer backbones, respectively (32,39,46). In contrast, amastigotes showed three IPC species, two of the same *m/z* as in promastigotes, but with *m/z* 806 and 808 more abundant in amastigotes and the *m/z* 778 greater in promastigotes (Fig. 6; (34). Amastigotes also displayed an additional unique species of *m/z* 808.6. To further explore their origins, we employed ESI/MS to determine the structures.

For the $[M – H]^-$ ion of IPC at *m/z* 778.6, the MS^2 spectra from both amastigotes and promastigotes contain a peak at *m/z* 598 resulting from the loss of inositol (Fig. 9A). MS^3 on m/z 598 originated from amastigotes (Fig. 9B) yielded ions of *m/z* 360 and 342, arising from loss of 16:0-FA as acid and ketene, respectively, together with ion of *m/z* 255 representing a 16:0 fatty acid carboxylate anion, leading to a final structure of d18:1/16:0-IPC. In contrast, MS^3 on m/z 598 originated from promastigotes (Fig. 9C) yielded ions of *m/z* 332 and 314 arising from loss of 18:0-FA as acid and ketene, respectively, together with the 18:0 fatty acid carboxylate anion ion at *m/z* 283, resulting in assignment of a d16:1/18:0-IPC structure (32,39). Interestingly,

and unlike promastigotes, the amastigote IPC ion of *m/z* 778.6 contains the same ceramide backbone as the abundant salvaged mammalian SM (Fig. 7).

For the amastigote IPC *m/z* 806.6 species, the MS^2 spectrum contained the ion *m/z* 626 arising from loss of inositol (Fig. 9A), which was further dissociated (MS^3) to ions of *m/z* 360 and 342 by loss of 18:0-FA as ketene and acid, respectively. The spectrum also contained the ion of *m/z* 283, representing a 18:0 fatty acid carboxylate anion (Fig. 9D). The combined structural information led to define the d18:1/18:0-IPC structure, which is identical to that previously determined for the promastigote IPC (*m/z* 806.6) (32). Lastly, MS^2 on the ion of *m/z* 808.6, the unique to amastigotes, gave rise to an ion of *m/z* 628 (loss of inositol) (Fig. 9A), which was further dissociated (MS^3) to ions of *m/z* 362 and 344 by loss of 18:0-FA as ketene and acid respectively, along with the 18:0 carboxylate anion of *m/z* 283 (Fig. 9E). These results readily defined a d18:0/18:0-IPC structure.

The above structural information of IPCs from amastigote and promastigote (summarized in Fig. 9A) indicates that IPC synthesis in amastigotes may arise through salvage, with two unique ceramide anchors not seen in promastigote IPCs. and is considered further in the discussion.

Discussion

Here we characterized IPC synthesis by *Leishmania major* across the infectious cycle, and through genetic deletion established a surprising lack of impact of IPC and *IPCS* knockouts on parasite biology and virulence in susceptible mouse infections. Our data suggest this likely reflects extensive salvage of host sphingolipids including sphingomyelin. We consider these findings in the context of SL uptake and metabolism, and their consequences towards efforts to target parasite SL metabolism in chemotherapy.

***Minimal impact of* IPCS *knockout on promastigotes* in vitro.** In contrast to other eukaryotic microbes, *IPCS*-null (*Δipcs*⁻) parasites could be readily obtained (Fig. 1), which as promastigotes appeared nearly normal, with only small differences in cell shape, growth and viability (Fig. 4A,B). *Δipcs*⁻ promastigotes lacked IPCS enzymatic activity (Figs. 2, S1), and both promastigotes and amastigotes lacked IPC (Figs. 3, 6), ruling out alternatives sources of IPC synthesis across the infectious cycle. We also confirmed that endogenously synthesized IPCS was insensitive to aureobasidin A, as seen with recombinant enzyme (Fig. 2) and mitigating a role for IPCS-interacting proteins (26,48). In all studies, ectopic re-expression of *IPCS* restored IPC synthesis and all other phenotypes tested (Figs. 3-5). IPCS activity consumes ceramide and PI to yield IPC and DAG, however the health of *Δipcs*⁻ suggests that perturbations of these substrates in this context likely has little deleterious effect during the infectious cycle. Provision of high levels of exogenous DAG had little effect on *Δipcs*⁻ but feeding SBs proved toxic, presumably due to excessive accumulation of SBs and/or ceramide in the absence of further metabolism as seen in *Leishmania* and fungi (38,49). *Δipcs*⁻ was strongly inhibited relative to WT when grown at pH 5 (Fig. 4D), however this effect was largely ameliorated at pH 5.5 or above (Supplemental Table 2). This is consistent with the survival of *Δipcs*⁻ in animal infections (Fig. 5), as the *Leishmania major* parasitophorous vacuole has a pH of 5.4 (50) which would only weakly impact *Δipcs*⁻. In these properties, *Leishmania* differs significantly from *Cryptococcus neoformans*, where *IPCS* is essential and IPCS-deficient organisms are hyper-susceptible to pH stress through an absence of DAG signaling (22).

Minimal impact of* IPCS *deletion on virulence and pathology. Distinct from other eukaryotic microbes, *Δipcs*⁻ *L. major* showed no defects in virulence as revealed by their ability to survive

and induce progressive pathology when inoculated into susceptible mice (Figs. 5, S4A), consistent with the findings *in vitro* with promastigotes where there was little change in properties expected to play significant role in amastigotes. In fact, lesion pathology was somewhat enhanced in the *Δipcs*⁻, as was the parasite burden (Fig. 5, S4B). Several studies have reported interactions between *Leishmania* and host ceramide impacting macrophage survival of the related species *L. donovani* (51,52). We did observe somewhat higher levels of ceramides in purified amastigotes relative to infected host tissue (Fig S5), and speculatively the modest hypervirulence seen with *L. major Δipcs*⁻ might arise from this.

Abundant salvage leads to predominance of SM over IPC in WT* Leishmania *amastigotes. *Leishmania* promastigotes can survive perfectly well without any cellular SLs (31,32), raising the possibility that the amastigote stage could likewise lack a requirement for SLs. However, *Leishmania* sp. are known to take up a variety of host lipids (53-55), and perhaps potential amastigote-stage SL requirements could be satisfied through uptake and metabolism of host SLs. MS analysis of purified amastigotes showed high levels of host SM in both WT and *Δipc*⁻, with SM estimated to be about 7-fold more abundant than parasite IPC (estimated previously to be present at about 10^8 molecules/amastigote) (34).

Thus host SM represents by far the most abundant salvaged SL within the parasite, even in WT amastigotes where it greatly predominates over IPC. This suggests that loss of IPC in *Δipcs*⁻ might result in only a slight reduction in total SLs, which might have little effect or be ameliorated by a small increase in SM salvage. Given the relative health and virulence of amastigotes lacking IPC, the question of why *Leishmania* continue to synthesize it at all now arises. Perhaps rather than contributing to bulk SL levels or metabolism, specific recognition of

IPC by host defenses could contribute to *Leishmania* pathology in some circumstances not tested here.

Metabolism of salvaged host SLs by* Leishmania *amastigotes. While the majority of salvaged SM remains intact in amastigotes, that further metabolism of acquired host SLs leading to parasite IPC synthesis occurs is mandated by the fact that *de novo* sphingoid base synthesis is shut down in amastigotes, a finding recapitulated in Δ*spt2*$^-$ amastigotes lacking serine palmitoyl transferase (32,34). Not only are IPC levels maintained in amastigotes, but amastigotes bear two IPCs with ceramide anchors not seen in promastigotes (d18:1/16:0-IPC and d18:0/18:0-IPC), with alterations in relative abundance as well (Fig. 9).

Several studies of murine host macrophages show that they elaborate a spectrum of SLs bearing anchors that could serve as a source for those present in amastigote IPC (46,47) (Table S3; a summary of these data is presented in Fig. 10). It can be seen that potential donors for the three amastigote IPC ceramide anchors can be found in both host SM and ceramides, or even through various SBs and ceramide synthesis (Fig. 10; the shading is based on the amastigote IPC anchor structures). Other SL possibilities may include host glucosylceramides which were not considered further here.

Focusing first on SM donors because of the massive uptake of host d18:1/16:0-SM, one potential route is through the potent sphingomyelinase / inositolphosphorylceramidase activity encoded by *Leishmania ISCL* (44,56-58) (Fig 10). Alternatively (and not exclusively), an *ISCL*-independent route could involve salvage of mammalian SBs or ceramides with related anchors directly (Fig. 10). Both routes are challenged by the *a priori* expectation that the ratio of the various amastigote IPC anchors would be expected to mirror that of the salvaged SL forms, from either *ISCL*-dependent or independent routes. However, while amastigote d18:1/16:0 IPC is the

least abundant IPC isoform, constituting less than 20% of total IPC, d18:1/16:0 SM is by far more abundant than other isoforms, constituting more than 80%, in either the parasite or the host (46,47) (Fig. 7, S7; Table S3). Factors that could contribute to these differences include differences in relative uptake of different SMs or ceramides, preferential salvage of host ceramides rather than ISCL-mediated degradation of SMs, or intrinsic differences in these activities with SMs or ceramides of differing anchor structure, for which there is currently little knowledge. Alternatively, an *ad hoc* hypothesis postulates there are two pools/routes of SL uptake, one emphasizing the abundant d18:1/16:0 SM, and the other more broadly acting across different IPC or ceramide anchor classes feeding into IPC synthesis (Fig. 10). Future studies will be required to address these interesting questions.

Interestingly and unlike *de novo* SL or IPC synthesis, the *ISCL* SMase activity is localized to the parasite mitochondrion where it is required for *Leishmania* virulence, albeit with some variation amongst parasite species or hosts (44,56). Beyond bulk catabolism, the *ISC1* fungal orthologs of *ISCL* play roles in mitochondrial metabolism, replication and SL signaling (59,60). Currently the molecular mechanism(s) by which SM or other SLs are acquired or partitioned into various metabolic pathways by *Leishmania* amastigotes is unknown, and unfortunately genetic approaches have been uninformative since no *Leishmania* mutants lacking SLs entirely have emerged.

Implications of the relative 'insignificance' of IPCS to chemotherapy. We did not anticipate that IPC or IPCS would not be essential at *any* point in the parasite infectious cycle, unlike pathogenic fungi where IPCS is an essential enzyme with considerable potential as a drug target. In this respect, our data do not provide much optimism for IPCS as a drug target in the *Leishmania* parasite. While some have reported activity of the yeast IPCS inhibitor aureobasidin

A, it has a high IC_{50} and is inactive against recombinant IPCS from trypanosomes and *Leishmania* as well as microsomal *Leishmania* IPCS activity (25,26) (Fig. 2). Whether new candidate inhibitors showing activity against cultured parasites (26-29) act 'on target' against *Leishmania* IPCS remains to be seen, although the health of the *Δipcs*⁻ mutant suggest this may be unlikely. *In vitro*, IPCS inhibitors may act synergistically with other compounds, although whether this extends to the *in vivo* situation with abundant SL salvage remains to be seen, in *Leishmania* or other pathogens known to take up host lipids.

Our studies thus provide a new perspective on *Leishmania* SL pathways, emphasizing the role of SM salvage from the host cell over *de novo* synthesis by the amastigote stage, additionally raising many interesting questions that will require further study. Instead, our findings with IPCS or previous studies with ISCL suggest that agents inhibiting SL uptake or catabolism in *Leishmania* may have more promise as chemotherapeutic agents.

Experimental Procedures

Molecular constructs. Molecular constructs containing 610 bp of 5' flanking (PCR amplified from WT genomic DNA by primers SMB 2590 and 2591; Table S1 contain the sequences of all oligonucleotides used) and 665 bp of 3' flanking (amplified by primers SMB 2592 and 2593) sequence flanking the *IPCS* ORF were joined by fusion PCR to the ORF for the selectable markers NEO (amplified by primers SMB2586 and 2587) or SAT (amplified by primers SMB 2588 and 2589). These constructs (pGEM T Easy-IPCS::ΔNEO, B5810, or pGEM T Easy-IPCS::ΔSAT, B6075) were linearized by digestion with EcoRI to expose the homologous ends prior to electroporation. To restore IPCS expression, the IPCS coding region (Lm35.4990) was

amplified by PCR using the primers SMB 3259 and 3260 and inserted into the pXG expression vector (61,62) yielding pXG-BSD-IPCS (B6235). All constructs were confirmed by sequencing.

***Leishmania* culture and transfection.** *Leishmania major* (LV39 clone 5, Rho/SU/59/P) was grown in M199 media supplemented with 10% fetal bovine serum, 12 mM $NaHCO_3$, 0.1 mM adenine, 7.6 mM hemin, 2 μg/ml biopterin, 20 μM Folic Acid, 1x RPMI Vitamin Mix, 2mM glutamine, 25 mM HEPES pH 6.8, 50 U/ml penicillin, and 50 μg/ml streptomycin (63) . Cell density was measured using a coulter counter (Becton Dickinson) and viability was determined by flow cytometry (Becton Dickinson) after staining with 5μg/ml propidium iodide. In some experiments supplements were added as indicated, or the pH was altered as shown in table S1 and MES or citrate buffers. Metacyclic cells were prepared by density purification or PNA-purification as described (40).

Transfections were performed by electroporation as previously described (64). To replace the first IPCS allele, transfection with the *IPCS:: ΔNEO* targeting fragment was performed; due to some media/serum concerns at the time these studies were undertaken, we had difficulty recovering transfectant colonies by our usual plating procedures. Thus, after electroporation and a 24 hr recovery period in 3 separate pools, clonal lines were obtained by limiting dilution in M199 medium containing 10 μg/ml neomycin and 500 μM EtN. The authenticity of several putative heterozygous transfectants (*IPCS / IPCS:: ΔNEO*) was confirmed by PCR. Correct integration was confirmed by using primers outside the flanking region and inside the drug marker (SMB2598/2600 5'Flank and SMB2608/2827 3'Flank). Several independent clonal lines were inoculated into susceptible BALB/c mice (10^7 parasites/footpad) and recovered after 1 month; such lines are referred to as M1 passage. Two such lines (WA and WB) were then transfected with the *IPCS:: ΔSAT* targeting fragment, resistant cells obtained

following growth in 8 μg/ml neomycin and 100 μg/ml nourseothricin, and clonal lines obtained by limiting dilution. The authenticity of potential homozygous Δ*ipcs*⁻ null mutants (formally *IPCS:: ΔNEO/IPCS:: ΔSAT*) was confirmed by PCR as described above using primers SMB 2598/2601 (5' flank) and SMB 2609/2827 (3' Flank). Several lines were inoculated into BALB/c mice as before. IPCS expression was restored in several Δ*ipcs*⁻ M1 transfectants (WAB, WAD, and WAE) by transfection with pXG-BSD-IPCS (B6235) to generate *ipcs::* Δ*NEO/ipcs::* Δ*SAT/+pXG-IPCS*, referred to as Δ*ipcs*⁻/+*IPCS*. As all transfectant and add-back lines showed similar behavior in preliminary tests, detailed studies are presented only for clone WAD (Δ*ipcs*⁻) or WADB (Δ*ipcs*⁻/+*IPCS*) unless otherwise stated.

Microsomal Preparation and Enzyme Assays. Microsomes were prepared by washing 4 x 10^8 promastigotes in PBS and homogenized by sonication in buffer (50mM MES, 50mM BIS-TRIS pH 6.25, 10mM EDTA, 100mM NaCl, 250 mM Sucrose, 300 nM aprotinin, 1 mM benzamidine, 1μg/ml chymostatin and pepstatin, 10 μM E64 and leupeptin, 10 mM NaF). Debris was removed by centrifugation at 1,000 x g for 10 min and the supernatant was then centrifuged at 100,000 x g for 90 minutes. The pellet was resuspended in minimal amounts of buffer (5 mM MES, 5 mM BIS_TRIS pH 6.25, 1 mM EDTA, 100 mM NaCl, 15 % glycerol, 300nM aprotinin, 1mM benzamidine, 1μg/ml chymostatin and pepstatin, 10 μM E64 and leupeptin, 1 mM NaF) with sonication then flash frozen. Protein content was determined by BCA assay using BSA standards.

Enzyme assays were performed in 100 μl IPCS assay buffer (100mM MES, 100mM BIS-TRIS pH 6.25, 5mM EDTA, 100mM NaCl, 300nM aprotinin, 1mM benzamidine, 1μg/ml chymostatin and pepstatin, 10 μM E64 and leupeptin, 1 mM NaF) Lipid substrates were dried by speedvac prior to resuspension is assay buffer, using 625 picomoles of L-α-phosphatidylinositol

from soy and 250 picomoles of NBD-C_6-Ceramide unless otherwise indicated. 25 μg of microsomal protein was added to the reactions which were incubated at 28°C for 60 minutes and terminated with 500 μl of 50 mM HCl in methanol. Lipids were extracted with 1.5 ml of chloroform and 463 μl of 1M NaCl. Samples were vortexed and centrifuged at 1,500 x g for 5 min. The upper phase was re-extracted with 750 μl of chloroform:methanol (43:7) and the combined lower phases were dried by nitrogen stream. Samples were resuspended in 50 μl of chloroform:methanol (2:1) and 5 μl were loaded on predeveloped Baker Si-250-PA 60 A silica gel TLC plates and developed using chloroform:methanol:water:ammonium hydroxide (28%)/65:30:3:2/v:v:v:v. Images were developed using Fuji FLA-5000 phosphoimager.

Lipid Extraction. Promastigotes were collected from 100 ml cultures and lesion amastigotes were harvested as described (65). Sphingolipids from log phase promastigotes or amastigotes were extracted using a modified Folch extraction. First, 2 x 10^8 cells were resuspended in 1.5 ml 25 mM Sodium Fluoride with 2 ml Methanol and sonicated. Next, 4 ml of chloroform was added; samples were vortexed and centrifuged at 1,800 x g for 15 minutes. The upper phase was re-extracted with 2.5 ml of chloroform:methanol (43:7), vortexed, and centrifuged. Combined lower phases were back extracted with 2 ml of 50 mM sodium fluoride and 2 ml of Methanol, vortexed, and centrifuged. The lower phase was dried by nitrogen stream and extracted again with chloroform:methanol:50mM sodium fluoride (4:2:1), vortexed, and centrifuged. The lower phase was again dried by nitrogen stream and resuspended in 1 ml of chloroform:methanol (1:1) for analysis by mass spectrometry.

Mass Spectrometry. ESI/MS analyses were performed on a Thermo Scientific (San Jose, CA) triple stage quadrupole (TSQ) Vantage EMR mass spectrometer with Xcalibur operating system. Lipid extracts (10uL each injection) were loop injection to the HESI-II probe in a Thermo

Scientific™ Ion Max ion source by a built-in syringe pump which delivered a constant flow of methanol at 20uL/min. The mass spectrometer was tuned to unit-mass resolution, and the heated capillary temperature was set to 280°C. The electrospray needle was set at 4.0 kV and 3.5 kV for positive-ion and negative-ion modes operation, respectively, and the skimmer was at ground potential. The mass resolution of both Q1 and Q3 was set at 0.6 Da at half peak height to obtain the product-ion scan, precursor ion scan and neutral loss scan (NLS) mass spectra, using a collision energy of 30-40 eV with target gas of Ar (1.3 mtorr) in the rf-only second quadrupole (Q2). The mass spectra were accumulated in the profile mode.

Mouse Virulence. Mouse handling and experimental procedures were carried out in strict accordance with the recommendations in the Guide for the Care and Use of Laboratory Animals of the United States National Institutes of Health. Animal studies were approved by the Animal Studies Committee at Washington University (protocol #20-0396) in accordance with the Office of Laboratory Animal Welfare's guidelines and the Association for Assessment and Accreditation of Laboratory Animal Care International.

Briefly, BALB/c or γ-IFN knockout C57BL/6 mice (γKO) were infected with 10^5 metacyclics purified by gradient centrifugation (40), and footpad lesion swelling measured weekly. At key points parasites were enumerated by limiting dilution assays (66), or lesions were excised for purification of amastigotes as described previously (34) .

Supporting information.

This article contains supporting information available on-line.

Acknowledgments.

We thank the members of our laboratory and Kai Zhang (Texas Tech University, Lubbock) for helpful discussions and providing access to MS data of purified WT amastigotes for confirmation of the results presented here. This manuscript was submitted posthumously on behalf of John Turk.

Author contributions.

FMK, PK, FH and SMB, conceptualization; FMK, PK, SH and FH, investigations, FMK, FH and SMB, writing.

Funding.

Supported by NIH Grant AI31078 to SMB and the Division of Infectious Diseases, Washington University (FMK). The Mass Spectrometry Resource of Washington University is supported by NIH grants P30DK020579, P30DK056341, and P41GM103422.

Conflict of interest.

The authors declare that they have no conflicts of interest with the contents of this article.

Abbreviations.

WT, wild-type *Leishmania major*; SM, sphingomyelin; IPC, inositolphorphorylceramide; IPCS, inositolphosphorylceramide synthase; SL, sphingolipid; SLS, sphingolipid synthase; SB, sphingoid (long-chain) base; PC, phosphatidyl choline; PI, phosphatidyl insotiol; PI-PLC, phosphatidyl inositol phospholipase C; NBD-Cer, (6-((N-(7-Nitrobenz-2-Oxa-1,3-Diazol-4-yl)amino)hexanoyl)Sphingosine); MS,mass spectrometry; ISCL, inositol phosphorylceramide phospholipase C-like; ESI/MS, electrospray ionization mass spectrometry. γKO, γ-interferon knockout C57BL/6 mice. Lipid species abbreviations follow those recommended by the Lipid Maps consortium (www.lipidmaps.org).

References

1. Alvar, J., Velez, I. D., Bern, C., Herrero, M., Desjeux, P., Cano, J., Jannin, J., and den Boer, M. (2012) Leishmaniasis worldwide and global estimates of its incidence. *PLoS One* **7**, e35671
2. Pigott, D. M., Bhatt, S., Golding, N., Duda, K. A., Battle, K. E., Brady, O. J., Messina, J. P., Balard, Y., Bastien, P., Pratlong, F., Brownstein, J. S., Freifeld, C. C., Mekaru, S. R., Gething, P. W., George, D. B., Myers, M. F., Reithinger, R., and Hay, S. I. (2014) Global distribution maps of the leishmaniases. *Elife* **3**, e28051
3. Banuls, A. L., Bastien, P., Pomares, C., Arevalo, J., Fisa, R., and Hide, M. (2011) Clinical pleiomorphism in human leishmaniases, with special mention of asymptomatic infection. *Clin Microbiol Infect* **17**, 1451-1461
4. Herwaldt, B. L. (1999) Leishmaniasis. *Lancet* **354**, 1191-1199
5. Mannan, S. B., Elhadad, H., Loc, T. T. H., Sadik, M., Mohamed, M. Y. F., Nam, N. H., Thuong, N. D., Hoang-Trong, B. L., Duc, N. T. M., Hoang, A. N., Elhusseiny, K. M., Minh, L. H. N., Quynh, T. T. H., Nghia, T. L. B., Mai Nhu, Y., Tieu, T. M., Hirayama, K., Huy, N. T., and Hamano, S. (2021) Prevalence and associated factors of asymptomatic leishmaniasis: a systematic review and meta-analysis. *Parasitol Int* **81**, 102229
6. WHO. (2010) Control of the Leishmaniasesa: WHO Expert Committee on the Control of Leishmaniases. *World Health Organization Technical Reports* **949**, 1-186
7. Singh, O. P., Hasker, E., Sacks, D., Boelaert, M., and Sundar, S. (2014) Asymptomatic *Leishmania* infection: a new challenge for *Leishmania* control. *Clin Infect Dis* **58**, 1424-1429
8. Croft, S. L., Sundar, S., and Fairlamb, A. H. (2006) Drug resistance in leishmaniasis. *Clin Microbiol Rev* **19**, 111-126
9. den Boer, M., Argaw, D., Jannin, J., and Alvar, J. (2011) Leishmaniasis impact and treatment access. *Clin Microbiol Infect* **17**, 1471-1477
10. Sangshetti, J. N., Khan, F. A. K., Kulkarni, A. K., Arote, R., and Patil, R. H. (2015) Antileishmanial drug discovery: comprehensive review of the last 10 years. *Royal Society of Chemistry* **5**, 32376-32415
11. Zhang, K., Bangs, J. D., and Beverley, S. M. (2010) Sphingolipids in parasitic protozoa. *Adv Exp Med Biol* **688**, 238-248

12. Mina, J. G. M., and Denny, P. W. (2018) Everybody needs sphingolipids, right! Mining for new drug targets in protozoan sphingolipid biosynthesis. *Parasitology* **145**, 134-147
13. Guan, X. L., and Maser, P. (2017) Comparative sphingolipidomics of disease-causing trypanosomatids reveal unique lifecycle- and taxonomy-specific lipid chemistries. *Sci Rep* **7**, 13617
14. Oskouian, B., and Saba, J. D. (2010) Cancer treatment strategies targeting sphingolipid metabolism. *Adv Exp Med Biol* **688**, 185-205
15. Koeller, C. M., and Heise, N. (2011) The Sphingolipid Biosynthetic Pathway Is a Potential Target for Chemotherapy against Chagas Disease. *Enzyme Res* **2011**, 648159
16. Suzuki, E., Tanaka, A. K., Toledo, M. S., Levery, S. B., Straus, A. H., and Takahashi, H. K. (2008) Trypanosomatid and fungal glycolipids and sphingolipids as infectivity factors and potential targets for development of new therapeutic strategies. *Biochim Biophys Acta* **1780**, 362-369
17. Hannun, Y. A., and Obeid, L. M. (2018) Sphingolipids and their metabolism in physiology and disease. *Nat Rev Mol Cell Biol* **19**, 175-191
18. Megyeri, M., Riezman, H., Schuldiner, M., and Futerman, A. H. (2016) Making Sense of the Yeast Sphingolipid Pathway. *J Mol Biol* **428**, 4765-4775
19. Kaneshiro, E. S., Jayasimhulu, K., and Lester, R. L. (1986) Characterization of inositol lipids from *Leishmania donovani* promastigotes: identification of an inositol sphingophospholipid. *J Lipid Res* **27**, 1294-1303
20. Harrison, P. J., Dunn, T. M., and Campopiano, D. J. (2018) Sphingolipid biosynthesis in man and microbes. *Nat Prod Rep* **35**, 921-954
21. Pinneh, E. C., Stoppel, R., Knight, H., Knight, M. R., Steel, P. G., and Denny, P. W. (2019) Expression levels of inositol phosphorylceramide synthase modulate plant responses to biotic and abiotic stress in *Arabidopsis thaliana*. *PLoS One* **14**, e0217087
22. Luberto, C., Toffaletti, D. L., Wills, E. A., Tucker, S. C., Casadevall, A., Perfect, J. R., Hannun, Y. A., and Del Poeta, M. (2001) Roles for inositol-phosphoryl ceramide synthase 1 (*IPC1*) in pathogenesis of *C. neoformans*. *Genes Dev* **15**, 201-212
23. Heidler, S. A., and Radding, J. A. (2000) Inositol phosphoryl transferases from human pathogenic fungi. *Biochim Biophys Acta* **1500**, 147-152

24. Sutterwala, S. S., Hsu, F. F., Sevova, E. S., Schwartz, K. J., Zhang, K., Key, P., Turk, J., Beverley, S. M., and Bangs, J. D. (2008) Developmentally regulated sphingolipid synthesis in African trypanosomes. *Mol Microbiol* **70**, 281-296
25. Denny, P. W., Shams-Eldin, H., Price, H. P., Smith, D. F., and Schwarz, R. T. (2006) The protozoan inositol phosphorylceramide synthase: a novel drug target that defines a new class of sphingolipid synthase. *J Biol Chem* **281**, 28200-28209
26. Sevova, E. S., Goren, M. A., Schwartz, K. J., Hsu, F. F., Turk, J., Fox, B. G., and Bangs, J. D. (2010) Cell-free synthesis and functional characterization of sphingolipid synthases from parasitic trypanosomatid protozoa. *J Biol Chem* **285**, 20580-20587
27. Figueiredo, J. M., Dias, W. B., Mendonca-Previato, L., Previato, J. O., and Heise, N. (2005) Characterization of the inositol phosphorylceramide synthase activity from *Trypanosoma cruzi*. *Biochem J* **387**, 519-529
28. Mina, J. G., Mosely, J. A., Ali, H. Z., Denny, P. W., and Steel, P. G. (2011) Exploring *Leishmania majo*r Inositol Phosphorylceramide Synthase (LmjIPCS): Insights into the ceramide binding domain. *Org Biomol Chem*
29. Mina, J. G., Mosely, J. A., Ali, H. Z., Shams-Eldin, H., Schwarz, R. T., Steel, P. G., and Denny, P. W. (2010) A plate-based assay system for analyses and screening of the *Leishmania major* inositol phosphorylceramide synthase. *Int J Biochem Cell Biol* **42**, 1553-1561
30. Norcliffe, J. L., Mina, J. G., Alvarez, E., Cantizani, J., de Dios-Anton, F., Colmenarejo, G., Valle, S. G., Marco, M., Fiandor, J. M., Martin, J. J., Steel, P. G., and Denny, P. W. (2018) Identifying inhibitors of the *Leishmania* inositol phosphorylceramide synthase with antiprotozoal activity using a yeast-based assay and ultra-high throughput screening platform. *Sci Rep* **8**, 3938
31. Denny, P. W., Goulding, D., Ferguson, M. A., and Smith, D. F. (2004) Sphingolipid-free *Leishmania* are defective in membrane trafficking, differentiation and infectivity. *Mol Microbiol* **52**, 313-327
32. Zhang, K., Showalter, M., Revollo, J., Hsu, F. F., Turk, J., and Beverley, S. M. (2003) Sphingolipids are essential for differentiation but not growth in *Leishmania*. *Embo J* **22**, 6016-6026

33. Zhang, K., Pompey, J. M., Hsu, F. F., Key, P., Bandhuvula, P., Saba, J. D., Turk, J., and Beverley, S. M. (2007) Redirection of sphingolipid metabolism toward *de novo* synthesis of ethanolamine in *Leishmania*. *Embo J* **26**, 1094-1104
34. Zhang, K., Hsu, F. F., Scott, D. A., Docampo, R., Turk, J., and Beverley, S. M. (2005) *Leishmania* salvage and remodelling of host sphingolipids in amastigote survival and acidocalcisome biogenesis. *Mol Microbiol* **55**, 1566-1578
35. Ali, H. Z., Harding, C. R., and Denny, P. W. (2011) Endocytosis and Sphingolipid Scavenging in *Leishmania mexicana* Amastigotes. *Biochem Res Int* **2012**, 691363
36. Winter, G., Fuchs, M., McConville, M. J., Stierhof, Y. D., and Overath, P. (1994) Surface antigens of *Leishmania mexicana* amastigotes: characterization of glycoinositol phospholipids and a macrophage-derived glycosphingolipid. *J Cell Sci* **107**, 2471-2482
37. Cruz, A., Coburn, C. M., and Beverley, S. M. (1991) Double targeted gene replacement for creating null mutants. *Proc Natl Acad Sci U S A* **88**, 7170-7174
38. Hannun, Y. A., and Obeid, L. M. (2002) The Ceramide-centric universe of lipid-mediated cell regulation: stress encounters of the lipid kind. *J Biol Chem* **277**, 25847-25850
39. Hsu, F. F., Turk, J., Zhang, K., and Beverley, S. M. (2007) Characterization of inositol phosphorylceramides from *Leishmania major* by tandem mass spectrometry with electrospray ionization. *J Am Soc Mass Spectrom* **18**, 1591-1604
40. Spath, G. F., and Beverley, S. M. (2001) A lipophosphoglycan-independent method for isolation of infective *Leishmania* metacyclic promastigotes by density gradient centrifugation. *Exp Parasitol* **99**, 97-103
41. Subramanya, S., and Mensa-Wilmot, K. (2010) Diacylglycerol-stimulated endocytosis of transferrin in trypanosomatids is dependent on tyrosine kinase activity. *PLoS One* **5**, e8538
42. Lemercier, G., Dutoya, S., Luo, S., Ruiz, F. A., Rodrigues, C. O., Baltz, T., Docampo, R., and Bakalara, N. (2002) A vacuolar-type H+-pyrophosphatase governs maintenance of functional acidocalcisomes and growth of the insect and mammalian forms of *Trypanosoma brucei*. *J Biol Chem* **277**, 37369-37376
43. Hsu, F. F., and Turk, J. (2000) Characterization of phosphatidylinositol, phosphatidylinositol-4-phosphate, and phosphatidylinositol-4,5-bisphosphate by electrospray ionization tandem mass spectrometry: a mechanistic study. *J Am Soc Mass Spectrom* **11**, 986-999

44. Zhang, O., Wilson, M. C., Xu, W., Hsu, F. F., Turk, J., Kuhlmann, F. M., Wang, Y., Soong, L., Key, P., Beverley, S. M., and Zhang, K. (2009) Degradation of host sphingomyelin is essential for *Leishmania* virulence. *PLoS Pathog* **5**, e1000692
45. Hsu, F. F., and Turk, J. (2000) Structural determination of sphingomyelin by tandem mass spectrometry with electrospray ionization. *J Am Soc Mass Spectrom* **11**, 437-449
46. Dennis, E. A., Deems, R. A., Harkewicz, R., Quehenberger, O., Brown, H. A., Milne, S. B., Myers, D. S., Glass, C. K., Hardiman, G., Reichart, D., Merrill, A. H., Jr., Sullards, M. C., Wang, E., Murphy, R. C., Raetz, C. R., Garrett, T. A., Guan, Z., Ryan, A. C., Russell, D. W., McDonald, J. G., Thompson, B. M., Shaw, W. A., Sud, M., Zhao, Y., Gupta, S., Maurya, M. R., Fahy, E., and Subramaniam, S. (2010) A mouse macrophage lipidome. *J Biol Chem* **285**, 39976-39985
47. Raetz, C. R., Garrett, T. A., Reynolds, C. M., Shaw, W. A., Moore, J. D., Smith, D. C., Jr., Ribeiro, A. A., Murphy, R. C., Ulevitch, R. J., Fearns, C., Reichart, D., Glass, C. K., Benner, C., Subramaniam, S., Harkewicz, R., Bowers-Gentry, R. C., Buczynski, M. W., Cooper, J. A., Deems, R. A., and Dennis, E. A. (2006) Kdo2-Lipid A of E*scherichia coli*, a defined endotoxin that activates macrophages via TLR-4. *J Lipid Res* **47**, 1097-1111
48. Sato, K., Noda, Y., and Yoda, K. (2009) Kei1: a novel subunit of inositolphosphorylceramide synthase, essential for its enzyme activity and Golgi localization. *Mol Biol Cell* **20**, 4444–4457
49. Zhang, O., Hsu, F. F., Xu, W., Pawlowic, M., and Zhang, K. (2013) Sphingosine kinase A is a pleiotropic and essential enzyme for *Leishmania* survival and virulence. *Mol Microbiol* **90**, 489-501
50. Spath, G. F., Schlesinger, P., Schreiber, R., and Beverley, S. M. (2009) A novel role for Stat1 in phagosome acidification and natural host resistance to intracellular infection by *Leishmania major*. *PLoS Pathog* **5**, e1000381
51. Ghosh, S., Bhattacharyya, S., Das, S., Raha, S., Maulik, N., Das, D. K., Roy, S., and Majumdar, S. (2001) Generation of ceramide in murine macrophages infected with *Leishmania donovani* alters macrophage signaling events and aids intracellular parasitic survival. *Mol Cell Biochem* **223**, 47-60
52. Ghosh, S., Bhattacharyya, S., Sirkar, M., Sa, G. S., Das, T., Majumdar, D., Roy, S., and Majumdar, S. (2002) *Leishmania donovani* suppresses activated protein 1 and NF-kappaB

activation in host macrophages via ceramide generation: involvement of extracellular signal-regulated kinase. *Infect Immun* **70**, 6828-6838

53. Zhang, K. (2021) Balancing *de novo* synthesis and salvage of lipids by *Leishmania* amastigotes. *Curr Opin Microbiol* **63**, 98-103
54. McConville, M. J., and Naderer, T. (2011) Metabolic pathways required for the intracellular survival of *Leishmania*. *Annu Rev Microbiol* **65**, 543-561
55. Schneider, P., Rosat, J. P., Ransijn, A., Ferguson, M. A., and McConville, M. J. (1993) Characterization of glycoinositol phospholipids in the amastigote stage of the protozoan parasite *Leishmania major*. *Biochem J* **295**, 555-564
56. Pillai, A. B., Xu, W., Zhang, O., and Zhang, K. (2012) Sphingolipid degradation in *Leishmania* (*Leishmania*) *amazonensis*. *PLoS Negl Trop Dis* **6**, e1944
57. Xu, W., Xin, L., Soong, L., and Zhang, K. (2011) Sphingolipid degradation by Leishmania major is required for its resistance to acidic pH in the mammalian host. *Infect Immun* **79**, 3377-3387
58. Zhang, O., Xu, W., Balakrishna Pillai, A., and Zhang, K. (2012) Developmentally regulated sphingolipid degradation in *Leishmania major*. *PLoS One* **7**, e31059
59. Matmati, N., Hassan, B. H., Ren, J., Shamssedine, A. A., Jeong, E., Shariff, B., Snider, J., Rodkaer, S. V., Chen, G., Mohanty, B. K., Zheng, W. J., Obeid, L. M., Rossel-Larsen, M., Faergeman, N. J., and Hannun, Y. A. (2020) Yeast Sphingolipid Phospholipase Gene ISC1 Regulates the Spindle Checkpoint by a CDC55-Dependent Mechanism. *Mol Cell Biol* **40**
60. Spincemaille, P., Matmati, N., Hannun, Y. A., Cammue, B. P., and Thevissen, K. (2014) Sphingolipids and mitochondrial function in budding yeast. *Biochim Biophys Acta* **1840**, 3131-3137
61. Goyard, S., and Beverley, S. M. (2000) Blasticidin resistance: a new independent marker for stable transfection of *Leishmania*. *Mol Biochem Parasitol* **108**, 249-252
62. Ha, D. S., Schwarz, J. K., Turco, S. J., and Beverley, S. M. (1996) Use of the green fluorescent protein as a marker in transfected *Leishmania*. *Mol Biochem Parasitol* **77**, 57-64
63. Goyard, S., Segawa, H., Gordon, J., Showalter, M., Duncan, R., Turco, S. J., and Beverley, S. M. (2003) An in vitro system for developmental and genetic studies of *Leishmania donovani* phosphoglycans. *Mol Biochem Parasitol* **130**, 31-42

64. Kapler, G. M., Coburn, C. M., and Beverley, S. M. (1990) Stable transfection of the human parasite *Leishmania major* delineates a 30-kilobase region sufficient for extrachromosomal replication and expression. *Mol Cell Biol* **10**, 1084-1094
65. Akopyants, N. S., Matlib, R. S., Bukanova, E. N., Smeds, M. R., Brownstein, B. H., Stormo, G. D., and Beverley, S. M. (2004) Expression profiling using random genomic DNA microarrays identifies differentially expressed genes associated with three major developmental stages of the protozoan parasite *Leishmania major*. *Mol Biochem Parasitol* **136**, 71-86
66. Titus, R. G., Marchand, M., Boon, T., and Louis, J. A. (1985) A limiting dilution assay for quantifying *Leishmania major* in tissues of infected mice. *Parasite Immunol.* **7**, 545-555

Figure Legends

Figure 1: Generation of *Δipcs*⁻ promastigotes.
(A) Schematic of planned replacements for *IPCS* with drug markers for nourseothricin (*SAT*), G418 (*NEO*) and expression construct pXG-IPCS with blasticidin (*BSD*) resistance. Arrows represent the location of primers used for PCR; Primers 1/4 and 3/2 tests for correct *NEO* 5'and 3' replacements; primers 1/6 and 5/2 test for correct *SAT* 5' and 3' replacement; primers 7/2 tests for WT *IPCS* and 7/8 test for the pXG-born *IPCS*. Primer 1, SMB 2598; 2, SMB 2827; 3, SMB 2600; 4, SMB 2608; 5, SMB 2609; 6, SMB 2601; 7, SMB 2607; and 8, SMB 1421; sequences can be found in Table S1. (B) PCR confirmation of parasite transfectants. *IPCS*::*NEO* replacement (lanes 1,2, primers 1+4, expected size 860bp; and 3+2, expected size 1024bp); planned *IPCS::SAT* replacement (lanes 3,4, primers 1+6, expected size 849bp; and 5+2 , expected size 933bp); WT *IPCS* (lane 5, primers 7+2, expected size 882bp); and pXG-BS-IPCS (lane 6, primers 7+8, expected size 124bp).

Figure 2: Enzymatic characterization of IPCS activity and its absence in Δ*ipcs*⁻ promastigotes.
(A) NBD-IPC formation in complete reactions or in the absence of key substrates, microsomes, inhibitors or enzymatic treatments as indicated. (B) Quantitation of NBD-IPC formation by microsomes from WT, Δ*ipcs*⁻ or Δ*ipcs*⁻/+*IPCS* parasites. Primary TLC data can be found in Fig. S1.

Figure 3: Absence of IPC in Δ*ipcs*⁻ *Leishmania*. The figure shows the ESI/MS spectrum (negative ion mode) obtained with lipid preparations from logarithmic growth phase WT, Δ*ipcs*⁻, or Δ*ipcs*⁻/+*IPCS* promastigotes.

Figure 4: Phenotypic characterization of Δ*ipcs*⁻ promastigotes *in vitro*. (A), growth; (B), Propidium iodide exclusion (viability); (C), growth in the presence of 2 μM 3-keto-dihydrosphingosine; and (D), growth at pH 5.0 (MES buffer). All parasites were propagated in

standard M199 culture media at 25º C. Lines tested are WT (●), Δ*ipcs*⁻ (○), or Δ*ipcs*⁻/+IPCS (▼).

Figure 5: Δ*ipcs*⁻ promastigotes are fully virulent in susceptible mice. 10^5 purified metacyclic parasites were inoculated into the footpad of Balb/C mice and the lesion size measured. Data from a representative experiment is shown, with the average and standard deviation for groups of 4 mice; simple linear regression determined significantly different slopes between groups ($p < 0.0001$); combined data from 4 separate experiments show similar trends and are provided in Fig. S4A. Lines tested are WT (●), Δ*ipcs*⁻ (○), or Δ*ipcs*⁻/+IPCS (▼).

Figure 6: ESI/MS analysis of IPCs from purified amastigotes and infected tissue. Spectra were obtained by a triple stage quadrupole instrument applying precursor scan of 241 in the negative ion mode that focuses on IPCs and inositol phospholipid species in the lipid extracts. Samples were prepared from (A) purified WT amastigotes, (B) purified Δ*ipcs*⁻ amastigotes (clone WAE), and (C) total infected WT footpad lesions. γKO mice were used in the studies shown; similar findings with BALB/c hosts are shown in Figs. S5 and S6. Abbreviations: d16:1/18:0-IPC, phosphoryl inositol N-stearoylhexadecesphing-4-enine); d18:1/18:0-IPC, phosphoryl inositol N-stearoylsphingosine; d18:0/18:0-IPC, phosphoryl inositol N-stearoylsphinganine.

Figure 7: ESI/MS analysis of SMs from purified amastigotes and infected tissues. Spectra were acquired in the positive ion mode showing the [M + Na]+ ions of PC (labeled in red), SM (blue), PE (green) and TG (purple). Lipids were prepared from (A) purified WT amastigotes, (B) purified Δ*ipcs*⁻ amastigotes (clone WAE), and (C) total WT infected footpad lesions. γKO host mice were used in the studies shown; similar findings with BALB/c hosts are shown in Fig. S7. Abbreviations: d18:1/16:0-SM, N-palmitoyl-octadecesphing-4-enine-1-phosphocholine; PC, phosphatidylcholine; PE, phosphatidylethanolamine; SM, sphingomyelin; TG, triacylglycerol.. For phospholipids (PL) designation: A/B-PL illustrates A: combined number of carbon chainc of the fatty acid (FA) attached to glycerol backbone; B: total number of unsaturated bonds of FA substituents.

Figure 8: Relative abundance of WT amastigote SM and IPC. Internal standards **(**10 nmol d18:1/12:0-SM and 2 nmol of dipalmitoyol phosphoinositol) were added to WT amastigote samples, and lipids were extracted and analyzed by ESI/MS in the positive ion mode (panel A) or negative ion mode (panel B) to compare the relative amounts of SM and IPC present in the same sample. This experiment was repeated a second time with similar results.

Figure 9: Characterization of IPC ceramide anchors. (A), Summary of ESI/MS fragmentation results and deduced ceramide anchor structures. (B,C), MS^3 analysis of the IPC *m/z* 778.6 → *m/z* 598 ceramide moiety from amastigotes (B) or promastigotes (C). Notably the deduced amastigote IPC anchor is the same as mammalian d18:1/16:0-SM. (D), MS^3 analysis of the IPC m/z 806.6 →*m/z* 626 ceramide moiety from amastigotes (promastigotes were previously shown to contain the identical structure (32). (E), MS^3 analysis of the IPC *m/z* 808.6 → *m/z* 628 ceramide moiety from amastigotes (Promastigotes lack this IPC species). Fragments derived from the fatty acid moiety are highlighted or circled in blue, while SB-derived moieties (acid or ketene as described in the text) are highlighted or circled in red.

Figure 10: Summary of relevant SL structures and relative abundances in *Leishmania* amastigotes and murine host macrophages, and potential salvage and metabolic routes. *Leishmania* amastigotes lack *de novo* sphingoid base (SB) synthesis so SL synthetic and/or salvage pathways are shown starting at this point. The spectrum of SLs considered is restricted to C16/18 SLs relevant to IPC synthesis, and arises from this work or published data (46,47) (Table S3). The structures of ceramides or the ceramide anchor of SMs and IPCs is shown, with larger font heights signifying approximate relative abundance. The host ceramide or SM anchors are colored to match those of the *Leishmania* IPCs to facilitate discussion about potential host origins. Question marks indicate lack of information about the relative role of the indicated pathway in IPC synthesis. The heavy dashed black arrow marks the highly abundant d18:1/16:0-SM in both *Leishmania* amastigotes and the host, and is discussed further in the text.

Supporting information.

"Inositol Phosphorlyceramide Synthase null *Leishmania major* (Δ*ipcs*⁻) are viable and virulent in animal infections where salvage of host sphingomyelin predominates"

F. Matthew Kuhlmann, Phillip Key, Suzanne Hickerson, John Turk, Fong-Fu Hsu, and Stephen M. Beverley

Materials included.

Supplemental Table S1. Oligonucleotides used

Supplemental Table S2. Δ*ipcs*⁻ is strongly inhibited below pH 5.5

Supplemental Table S3. Summary of C16 and C18 species in mammalian macrophages.

Supplemental Figure S1. Representative TLC data relevant to enzymatic characterization of IPCS activity from purified microsomes, and its absence in Δ*ipcs*⁻ promastigotes**.**

Supplemental Figure S2. Phenotypic characterizations of WT and Δ*ipcs*⁻ mutant *L. major* propagated in M199 medium *in vitro*.

Supplemental Figure S3. Accumulation of phytoceramide in Δ*ipcs*⁻ parasites grown in the presence of phytosphingosine.

Supplemental Figure S4. *Δipcs*- remains highly virulent in animal infections

Supplemental Figure S5. ESI/MS spectra (negative ion mode) for purified amastigotes or infected mouse tissue.

Supplemental Figure S6. ESI/MS spectra from -241 parent ion scan (negative ion mode) for purified amastigotes or infected mouse tissue.

Supplemental Figure S7. ESI/MS spectra (positive ion mode) for purified amastigotes or infected mouse tissue.

Please note that due to their size, Figs S5-7 are included as separate on-line files.

Supplemental Table 1. Oligonucleotides used in this work.

Primer	Sequence (5'-3')	Purpose
SMB2586	CGACTCCCCCTCTCACCGCGGCCACCATGGGATCGGCCATTGAACAAGATGG	forward fusion primer to amplify *NEO* marker
SMB2587	GAGGTATCTCCTTGATGGGGTTTCAGAAGAACTCGTCAAGAAGGCG	reverse fusion primer to amplify *NEO* marker
SMB2588	CGACTCCCCCTCTCACCGCGGCCACCATGAAGATTTCGGTGATCCCTGAGCAGG	forward fusion primer to amplify *SAT* marker
SMB2589	GAGGTATCTCCTTGATGGGGTTTTAGGCGTCATCCTGTGCTCCCGAGAACC	reverse fusion primer to amplify SAT marker
SMB2590	CGTGCGGCTGCTTGTTTCTTACTTCTG	forward fusion primer to amplify 5' flanking region of *IPCS*
SMB2591	GGTGGCCGCGGTGAGAGGGGGAGTCG	reverse fusion primer to amplify 5' flanking region of *IPCS*
SMB2592	AACCCCATCAAGGAGATACCTC	forward fusion primer to amplify 3' flanking region of *IPCS*
SMB2593	CCAAGTCCGCGCAAAGATACACCTACA	reverse fusion primer to amplify 3' flanking region of *IPCS*
SMB3259	gagtggagatctGCCATGACGAGTCACGTGACAGCGCACG	forward primer to amplify *IPCS* adding BglII site
SMB3260	gaactaagatctTTAGTGCTCAGGCAAAGCCGCCGAC	reverse primer to amplify *IPCS* adding BglII site

Supplemental Table 2.

Growth of *Δipcs*⁻ *in vitro* is strongly inhibited below pH 5.5

The mean doubling time (hr) and 1 standard deviation (n = 4) of WT, *Δipcs*⁻ or *Δipcs*⁻/+*IPC* with the indicated pH and overlapping buffers is shown.

Buffer	pH	WT	*Δipcs*⁻	*Δipcs*⁻/+*IPC*
Citrate	5	19.7 ± 0.3	59.9 ± 18.6	20.8 ± 2.1
	5.5	10.8 ± 0.0	15.3 ± 3.7	11.3 ± 0.9
	6	9.5 ± 0.1	12.3 ± 1.8	10.1 ± 0.4
MES	5	66.8 ± 25.6	390.0 ± 119.3	35.0 ± 29.1
	5.5	20.1 ± 11.0	22.2 ± 9.9	46.6 ± 52.5
	6	8.8 ± 0.4	8.0 ± 4.2	9.2 ± 0.5
HEPES	6.8	8.4 ± 0.2	10.7 ± 0.1	9.3 ± 0.4

Supplemental Table 3.

Levels of C16 and C18 SLs present in several mammalian macrophage sources.

The average and range seen in thioglycolate-elicited, bone marrow-derived, and RAW264.7 macrophages is shown. Data were obtained from the Lipid Maps website (www.lipidmaps.org) (Raetz, Garrett et al. 2006, Dennis, Deems et al. 2010). Units are pM lipid / µg DNA.

Shading depicts an arbitrary cutoff for those SLs showing values >1.

Lipid Maps	Lipid Maps Analyte	Anchor	Average	Range
C16-18 Ceramides				
LMSP02010004	C16 Cer	d18:1/16:0-Cer	4.23	(2.48 - 6.82)
LMSP02050002	C16 CerP	d18:1/16:0-Cer-1-P	0.15	(0 - 0.42)
LMSP02050003	C16DH CerP	d18:0/16:0-Cer-1-P	0.00	(0 - 0.01)
LMSP02020001	C16DH Cer	d18:0/16:0-Cer	2.58	(0.63 - 4.25)
LMSP02010003	C18:1 Cer	d18:1/18:1-Cer	0.04	(0.03 - 0.06)
LMSP02020015	C18:1DH Cer	d18:0/18:1-Cer	0.24	(0.09 - 0.44)
LMSP02010006	C18 Cer	d18:1/18:0-Cer	0.19	(0.13 - 0.27)
LMSP02050004	C18 CerP	d18:1/18:0-Cer-1-P	0.06	(0 - 0.17)
LMSP02020008	C18DH Cer	d18:0/18:0-Cer	0.43	(0.28 - 0.61)
C16--C18 Glc-Ceramides				
LMSP0501AA03	C16 GlcCer	d18:1/16:0-GlcCer	6.29	(2.73 - 12.87)
LMSP0501AA04	C16DH GlcCer	d18:0/16:0-GlcCer	0.72	(0.18 - 1.53)
LMSP0501AA29	C18:1DH GlcCer	d18:0/18:1-GlcCer	0.00	(0 - 0.01)
LMSP0501AA27	C18:1 GlcCer	d18:1/18:1-GlcCer	0.01	(0 - 0.03)
LMSP0501AA19	C18DH GlcCer	d18:0/18:0-GlcCer	0.06	(0.01 - 0.11)
LMSP0501AA05	C18 GlcCer	d18:1/18:0-GlcCer	0.32	(0.11 - 0.46)
C16-C18 Sphingomyelins				
LMSP03010004	C16DH Sphingomyelin	d18:0/16:0-SM	29.34	(15.98 - 42.56)
LMSP03010003	C16 Sphingomyelin	d18:1/16:0-SM	191.94	(88.31 - 314.65)
LMSP03010020	C18DH Sphingomyelin	d18:0/18:0-SM	1.46	(0.59 - 2.76)
LMSP03010031	C18:1DH Sphingomyelin	d18:0/18:1-SM	6.84	(5.97 - 7.49)
LMSP03010029	C18:1 Sphingomyelin	d18:1/18:1-SM	0.69	(0.57 - 0.88)
LMSP03010001	C18 Sphingomyelin	d18:1/18:0-SM	6.52	(6.03 - 7.22)
Sphingoid bases				
LMSP01020001	Sphinganine	d18:0-SB	0.97	(0.07 - 2.62)
LMSP01050002	Sphinganine-P	d18:0-SB-1-P	23.57	(0.01 - 70.44)
LMSP01010001	Sphingosine	d18:1-SB	2.06	(0.76 - 3.12)
LMSP01050001	Sphingosine-P	d18:1-SB-1-P	0.91	(0.01 - 2.68)

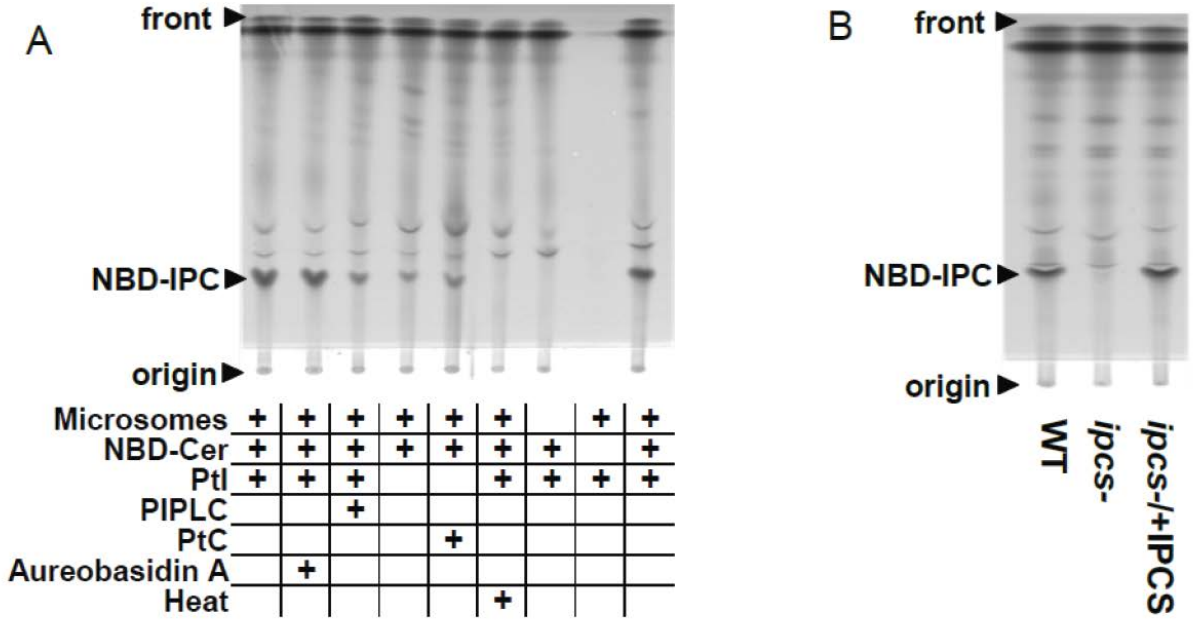

Figure S1: E**nzymatic characterization of IPCS activity from purified microsomes, and its absence in Δ*ipcs*⁻ promastigotes.**

The figure displays representative TLC separations used for the quantitative plots shown in Fig. 2.

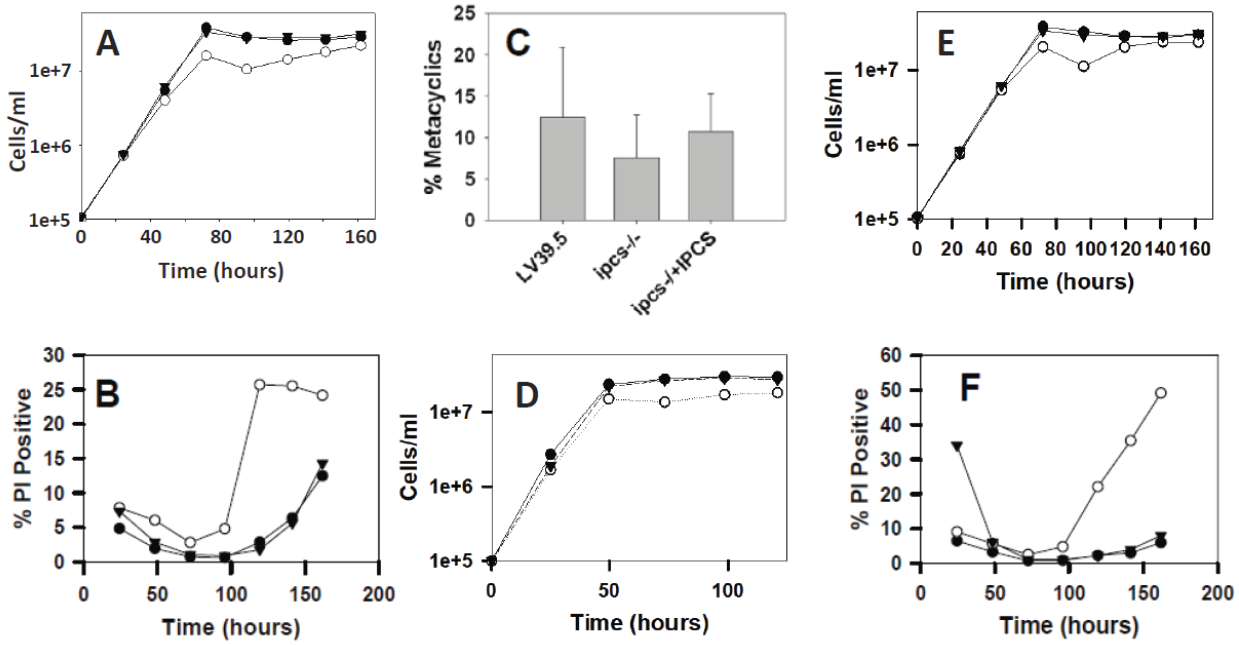

Figure S2: Phenotypic characterization of WT and Δ*ipcs*⁻ mutant *L. major* propagated in M199 medium *in vitro*.

(A, B), Growth and viability of parasites grown in 500 µM EtN. (C), Percent metacyclic observed at day 2 in stationary phase. (D), Growth of parasites at 33°C (at 37º all lines died). (E, F), growth and viability of parasites supplemented daily with 2 µM DAG.

Symbols are WT (●), Δ*ipcs*⁻ (○), or Δ*ipcs*⁻/+*IPCS* (▼).

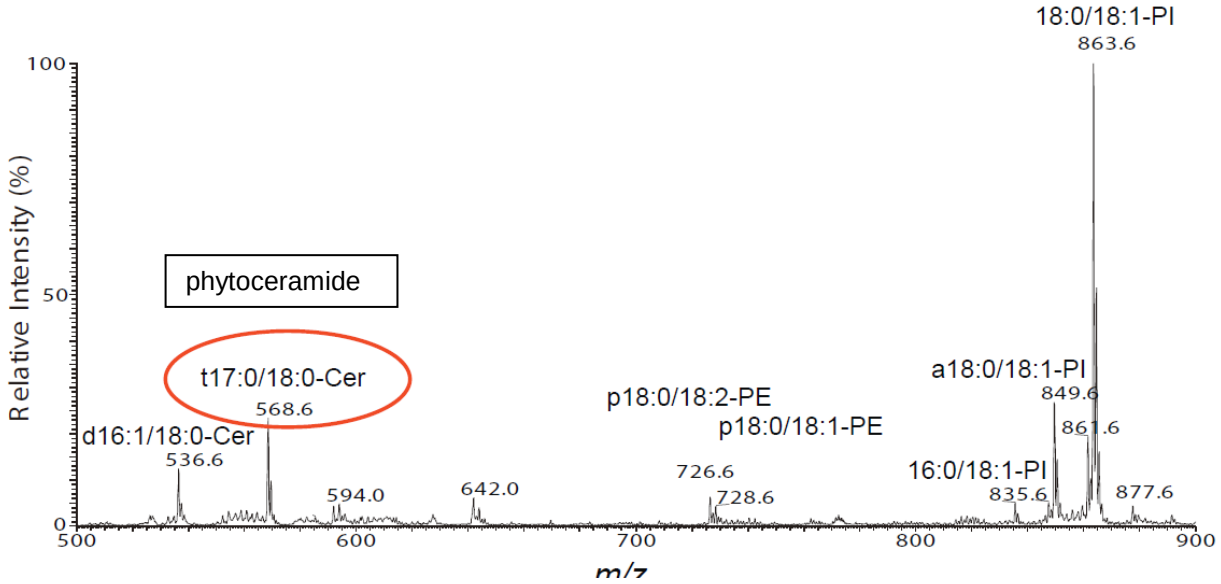

Figure S3: Accumulation of phytoceramide in Δ*ipcs*⁻ parasites grown in the presence of phytosphingosine.

The ESI/MS (negative ion mode) spectra obtained using purified lipids is shown. *In vitro* cultures of Δ*ipcs*⁻ parasites were inoculated at 1 x 10^6 cells/ml in M199 media containing 8 µM C17-phytosphingosine and grown 16 hr. The peak corresponding to phytoceramide (m/z 568) is circled. Nomenclature for individual lipid species is provided in the legends of Fig. 3 and Fig. 6.

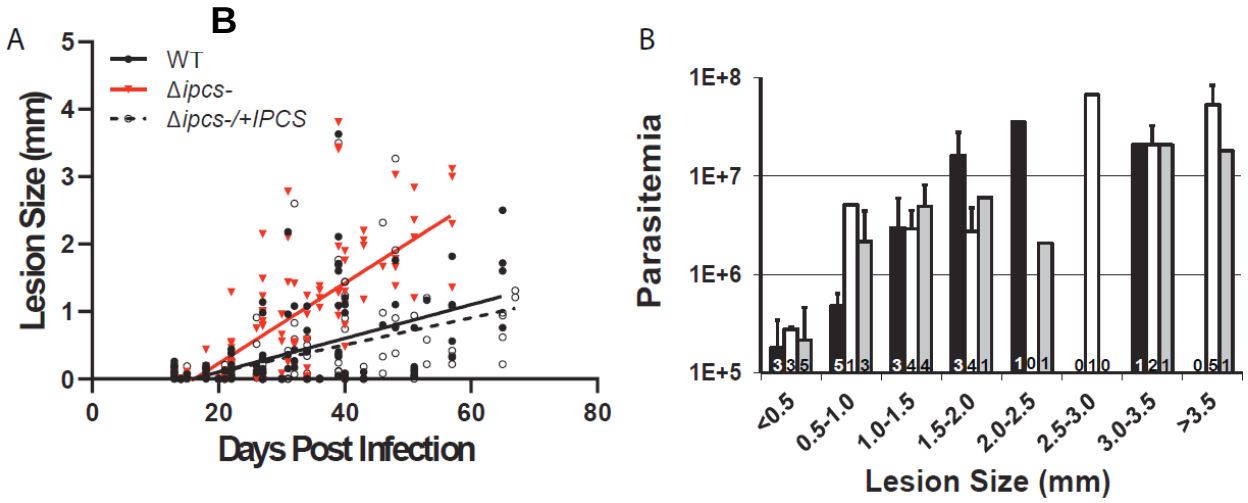

Figure S4. *Δipcs⁻* remains highly virulent in animal infections.

(A) Collected data from four independent experiments with 4-8 mice/group are plotted (a representative individual experiment is shown in Fig. 5). The lines (slopes) shown were calculated by simple linear regression showing significant differences between *Δipcs⁻* and WT or *Δipcs⁻/+IPCS* ($p < 0.0001$).

(B) Similar relationship between lesion size and parasite numbers in WT and mutant *L. major*. At various time points post-infection, lesions were excised and parasite numbers determined by limiting dilution. As not every experiment yielded lesions of a given size at the times measured for comparison, the small numbers within the bars denote the number of lesions, and the standard deviation is shown when possible. Parasite lines were WT (black bar), *Δipcs⁻* (white bar), and *Δipcs⁻/+IPCS* (gray bar) lesions.

Figure S5. ESI/MS spectra (negative ion mode) for purified amastigotes or infected mouse tissue. Total spectra are shown. (A), WT amastigotes purified from γKO mice infections. (B), infected lesion tissue from WT infected γKO mice. (C), *Δipcs*⁻ amastigotes (clone WAE) purified from γKO mice infections. (D), infected lesion tissue from *Δipcs*⁻ (clone WAE) infected γKO mice. (E), *Δipcs*⁻ amastigotes (clone WAB) purified from γKO mice infections. (F), infected lesion tissue from *Δipcs*⁻ (clone WAB) infected γKO mice. (G), WT amastigotes purified from BALB/c mice infections. (H), *Δipcs*⁻ amastigotes (clone WAE) purified from BALB/c mice infections. (I), *Δipcs*⁻ amastigotes (clone WAB) purified from BALB/c mice infections. Key ions as well as ones useful for comparative purposes were lined up across the panels; not marked is the peak at *m/z* 808.6 corresponding to d18:0/18.0-IPC. Lipid species abbreviations follow those recommended by the Lipid Maps consortium (www.lipidmaps.org).

Please note that due to the size, Fig. S5 can be found as a separate on-line file.

Figure S6. ESI/MS spectra from -241 parent ion scan (negative ion mode) for purified amastigotes or infected mouse tissue. Total spectra are shown. (A), WT amastigotes purified from γKO mice infections. (B), infected lesion tissue from WT infected γKO mice. (C), *Δipcs*⁻ amastigotes (clone WAE) purified from γKO mice infections. (D), infected lesion tissue from *Δipcs*⁻ (clone WAE) infected γKO mice. (E), *Δipcs*⁻ amastigotes (clone WAB) purified from γKO mice infections. (F), infected lesion tissue from *Δipcs*⁻ (clone WAB) infected γKO mice. (G), WT amastigotes purified from BALB/cmice infections. (H), *Δipcs*⁻ amastigotes (clone WAE) purified from BALB/c mice infections. (I), *Δipcs*⁻ amastigotes (clone WAB) purified from BALB/c mice infections. Key ions as well as ones useful for comparative purposes were lined up across the panels; not marked is the peak at *m/z* 808.6 corresponding to d18:0/18.0-IPC. Lipid species abbreviations follow those recommended by the Lipid Maps consortium (www.lipidmaps.org).

Please note that due to the size, Fig. S6 can be found as a separate on-line file.

Figure S7. ESI/MS spectra (positive ion mode) for purified amastigotes or infected mouse tissue. Total spectra are shown. (A), WT amastigotes purified from γKO mice infections. (B), infected lesion tissue from WT infected γKO mice. (C), *Δipcs*⁻ amastigotes (clone WAE) purified from γKO mice infections. (D), infected lesion tissue from *Δipcs*⁻ (clone WAE) infected γKO mice. (E), *Δipcs*⁻ amastigotes (clone WAB) purified from γKO mice infections. (F), infected lesion tissue from *Δipcs*⁻ (clone WAB) infected γKO mice. (G), WT amastigotes purified from BALB/c mice infections. (H), *Δipcs*⁻ amastigotes (clone WAE) purified from BALB/c mice infections. (I), *Δipcs*⁻ amastigotes (clone WAB) purified from BALB/c mice infections. Key ions as well as ones useful for comparative purposes were lined up across the panels.

Please note that due to the size, Fig. S7 can be found as a separate on-line file.

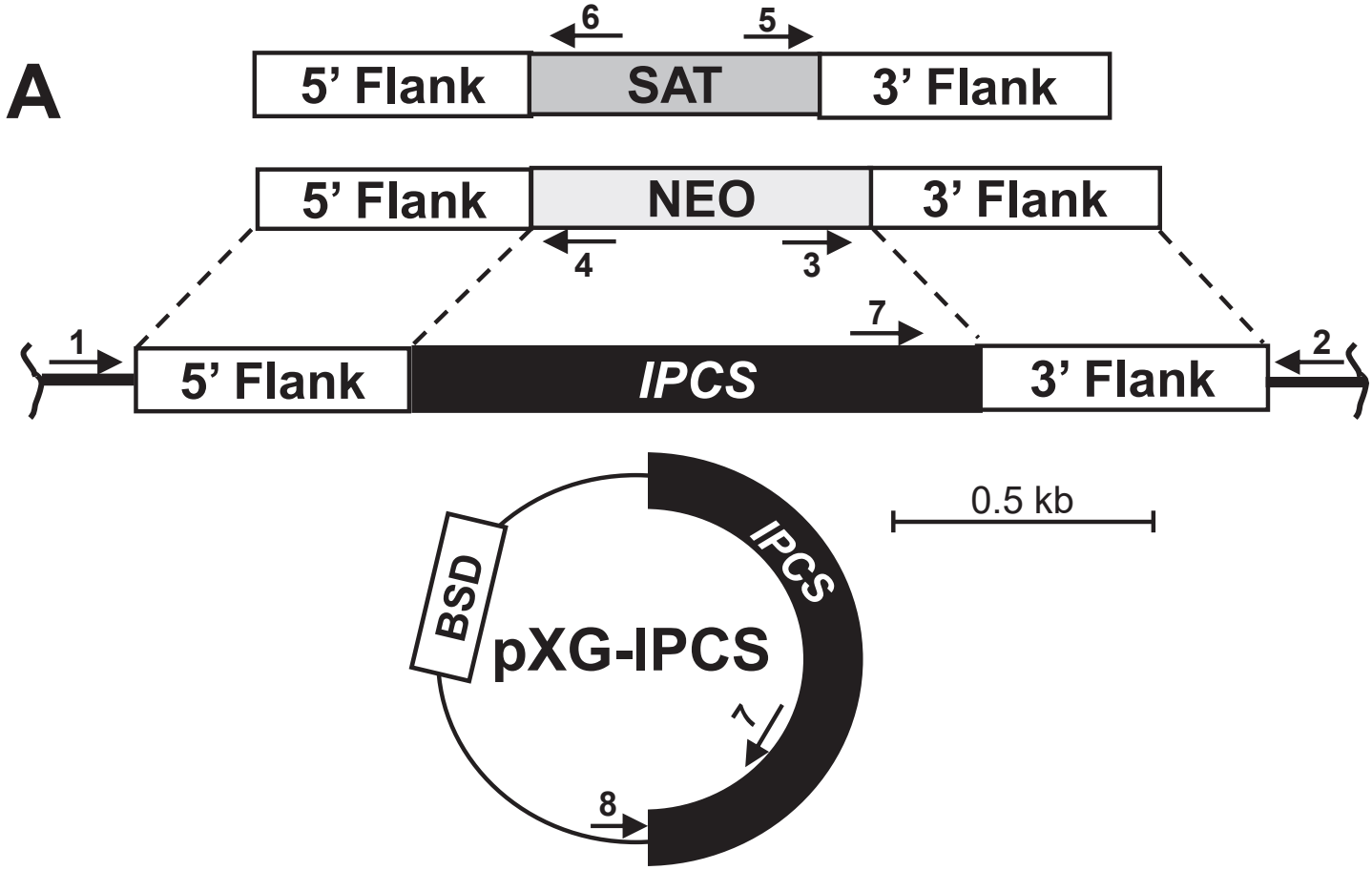
A
6
5
5' Flank
SAT
3' Flank
5' Flank
NEO
3' Flank
4
3
7
1
2
5' Flank
IPCS
3' Flank
0.5 kb
BSD
IPCS
pXG-IPCS
8

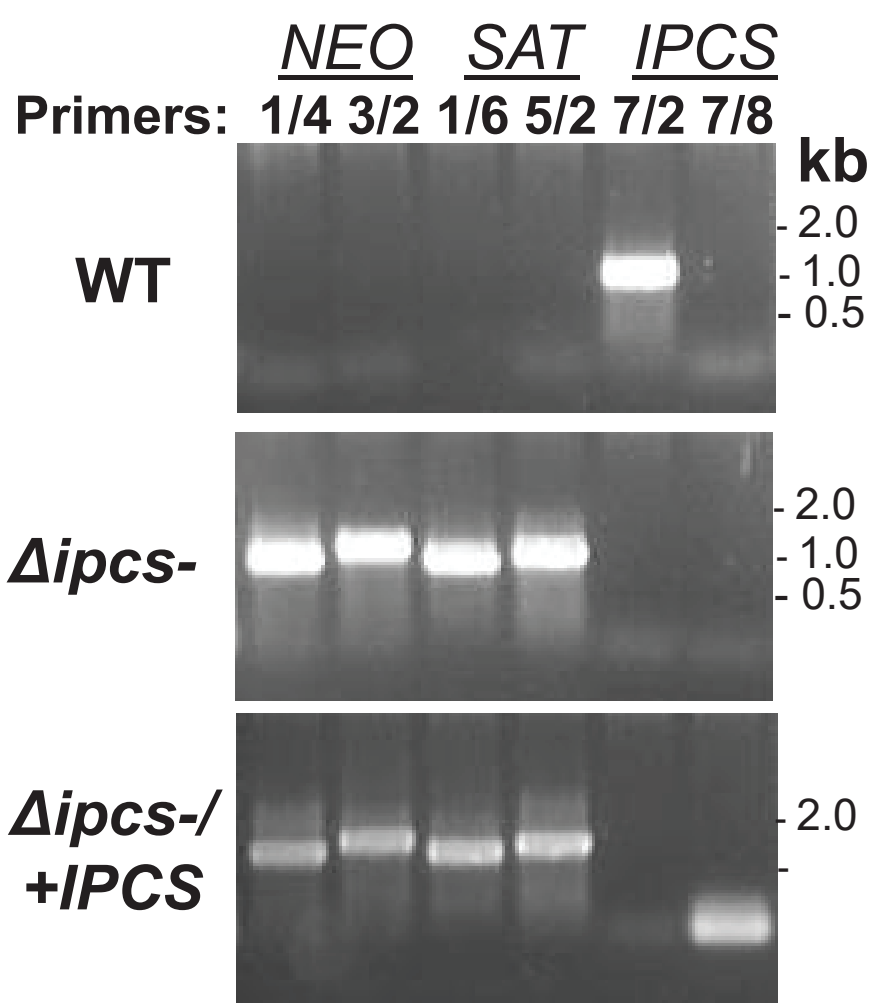
B
NEO
SAT
IPCS
Primers: 1/4 3/2 1/6 5/2 7/2 7/8
kb
WT
2.0
1.0
0.5
Δipcs-
2.0
1.0
0.5
Δipcs-/
+IPCS
2.0

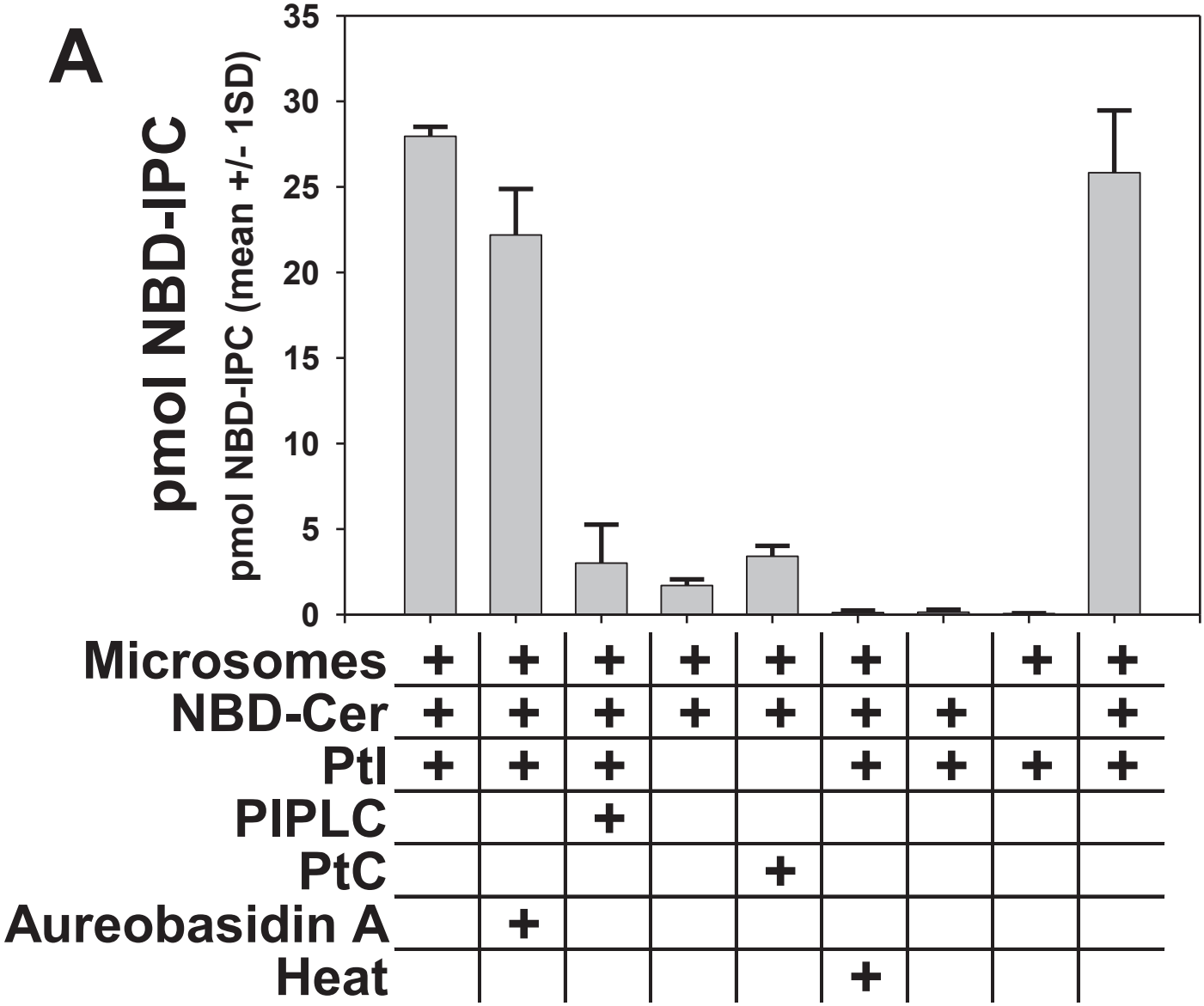
A
pmol NBD-IPC
pmol NBD-IPC (mean +/- 1SD)
35
30
25
20
15
10
5
0
Microsomes
NBD-Cer
PtI
PIPLC
PtC
Aureobasidin A
Heat

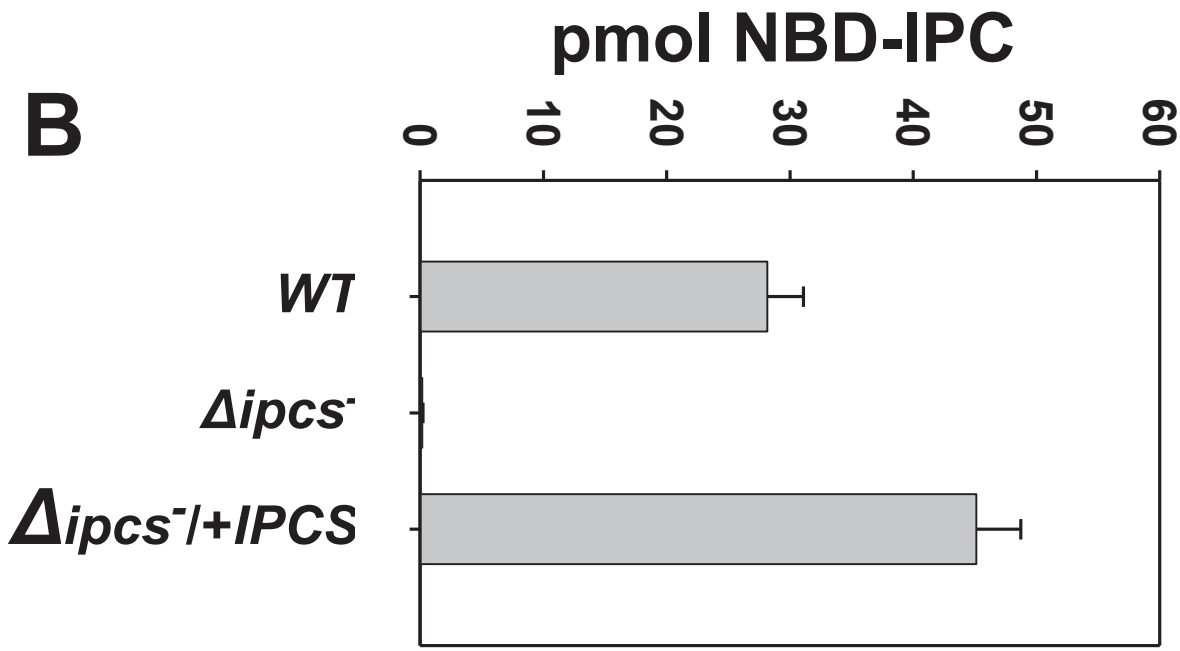
B
pmol NBD-IPC
0
10
20
30
40
50
60
WT
Δipcs-
Δipcs-/+IPCS

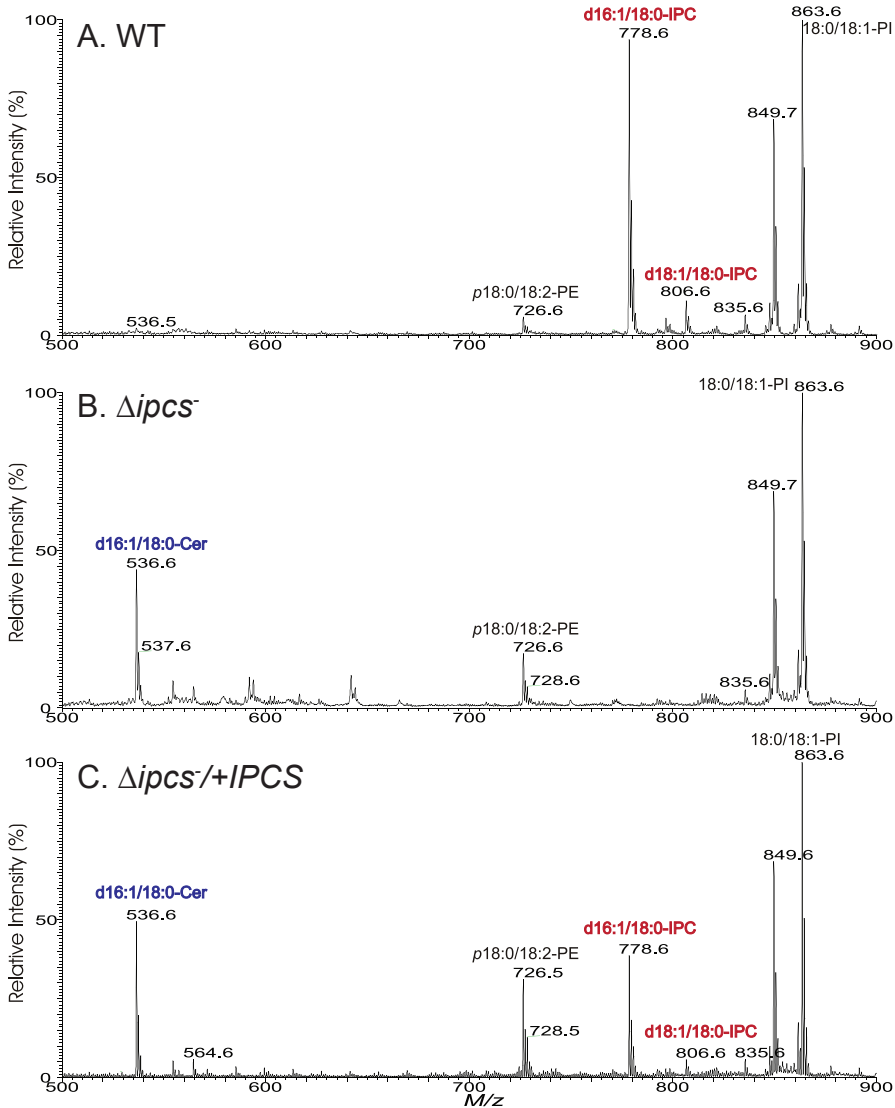
A. WT
d16:1/18:0-IPC
778.6
863.6
18:0/18:1-PI
849.7
d18:1/18:0-IPC
806.6
835.6
p18:0/18:2-PE
726.6
536.5
B. Δipcs⁻
18:0/18:1-PI 863.6
849.7
d16:1/18:0-Cer
536.6
537.6
p18:0/18:2-PE
726.6
728.6
835.6
C. Δipcs⁻/+IPCS
18:0/18:1-PI
863.6
849.6
d16:1/18:0-Cer
536.6
d16:1/18:0-IPC
778.6
p18:0/18:2-PE
726.5
728.5
d18:1/18:0-IPC
806.6
835.6
564.6
Relative Intensity (%)
100
50
0
500
600
700
800
900
M/z

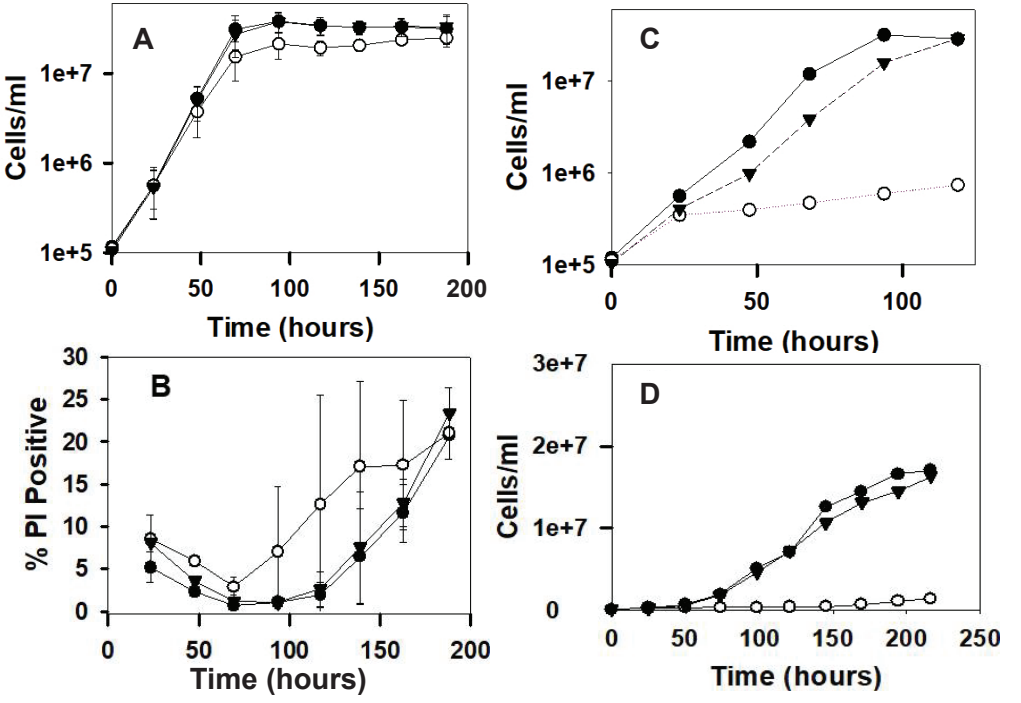
A
Cells/ml
1e+7
1e+6
1e+5
0
50
100
150
200
Time (hours)
C
Cells/ml
1e+7
1e+6
1e+5
0
50
100
Time (hours)
B
% PI Positive
30
25
20
15
10
5
0
0
50
100
150
200
Time (hours)
D
Cells/ml
3e+7
2e+7
1e+7
0
0
50
100
150
200
250
Time (hours)

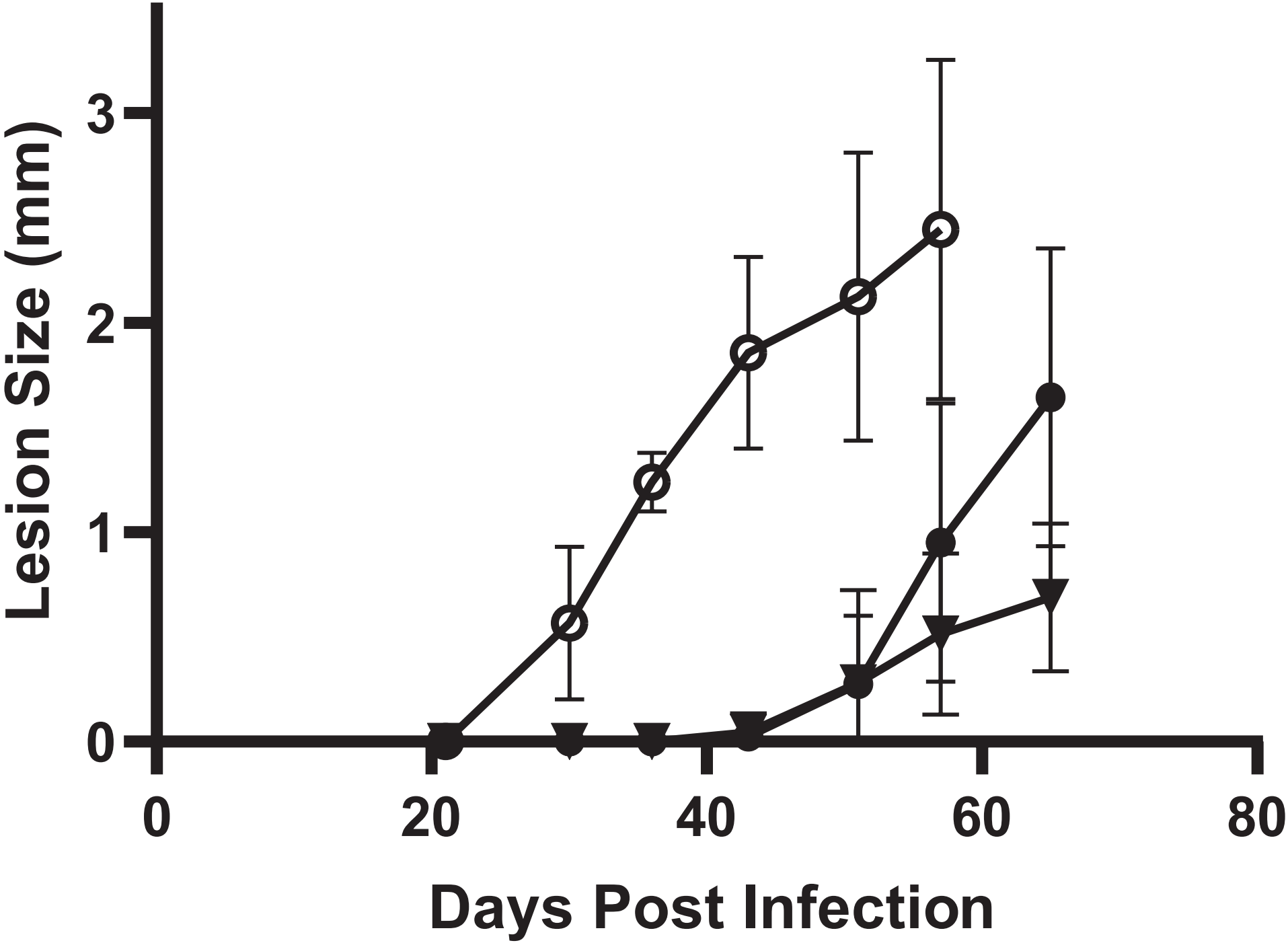
Lesion Size (mm)
3
2
1
0
0
20
40
60
80
Days Post Infection

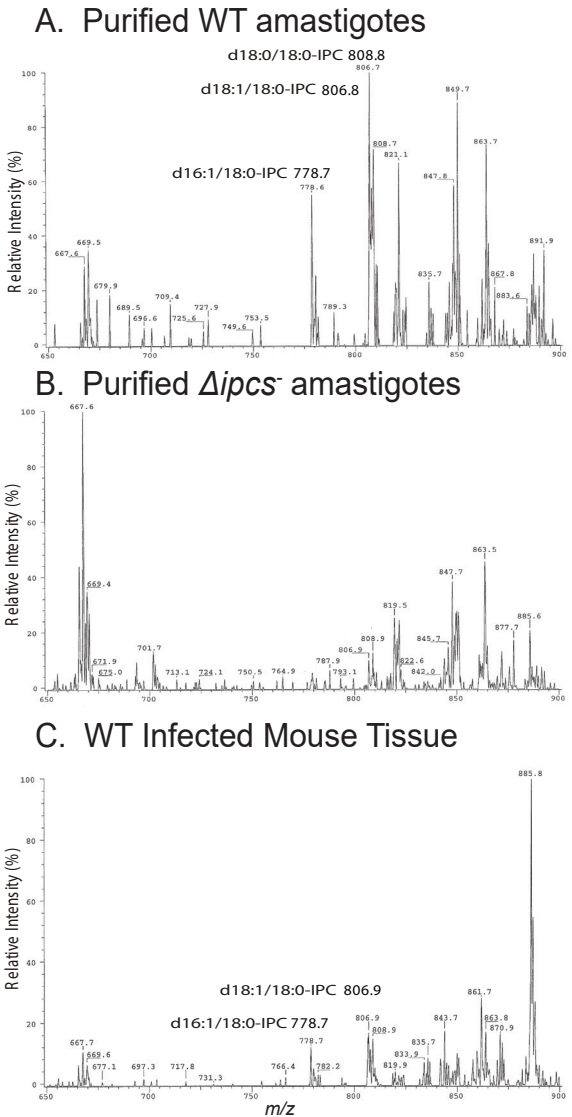
A. Purified WT amastigotes
d18:0/18:0-IPC 808.8
d18:1/18:0-IPC 806.8
d16:1/18:0-IPC 778.7
Relative Intensity (%)
B. Purified Δipcs⁻ amastigotes
Relative Intensity (%)
C. WT Infected Mouse Tissue
d18:1/18:0-IPC 806.9
d16:1/18:0-IPC 778.7
Relative Intensity (%)
m/z

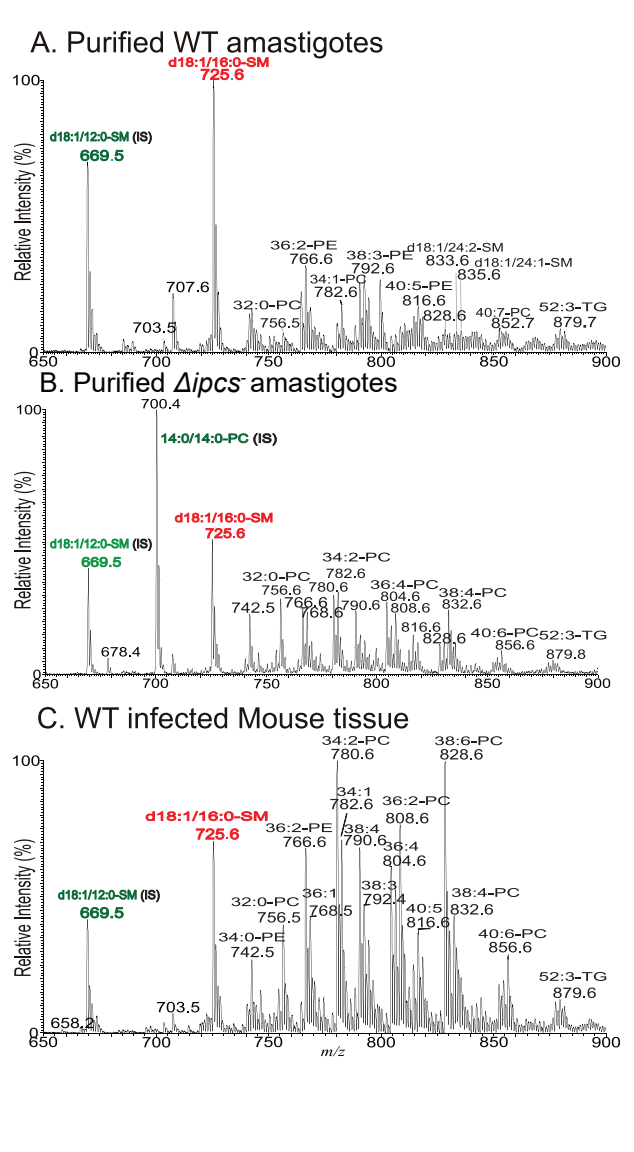
A. Purified WT amastigotes
d18:1/16:0-SM
725.6
d18:1/12:0-SM (IS)
669.5
36:2-PE
766.6
38:3-PE
792.6
d18:1/24:2-SM
833.6
d18:1/24:1-SM
835.6
34:1-PC
782.6
40:5-PE
816.6
828.6
707.6
32:0-PC
756.5
703.5
40:7-PC
852.7
52:3-TG
879.7
Relative Intensity (%)
B. Purified Δipcs⁻ amastigotes
700.4
14:0/14:0-PC (IS)
d18:1/16:0-SM
725.6
d18:1/12:0-SM (IS)
669.5
34:2-PC
782.6
32:0-PC
756.6
780.6
36:4-PC
804.6
38:4-PC
832.6
742.5
766.6
768.6
790.6
808.6
816.6
828.6
40:6-PC
856.6
52:3-TG
879.8
678.4
Relative Intensity (%)
C. WT infected Mouse tissue
34:2-PC
780.6
38:6-PC
828.6
34:1
782.6
36:2-PC
808.6
d18:1/16:0-SM
725.6
36:2-PE
766.6
38:4
790.6
36:4
804.6
d18:1/12:0-SM (IS)
669.5
36:1
768.5
38:3
792.4
38:4-PC
832.6
32:0-PC
756.5
40:5
816.6
34:0-PE
742.5
40:6-PC
856.6
52:3-TG
879.6
703.5
658.2
Relative Intensity (%)
m/z

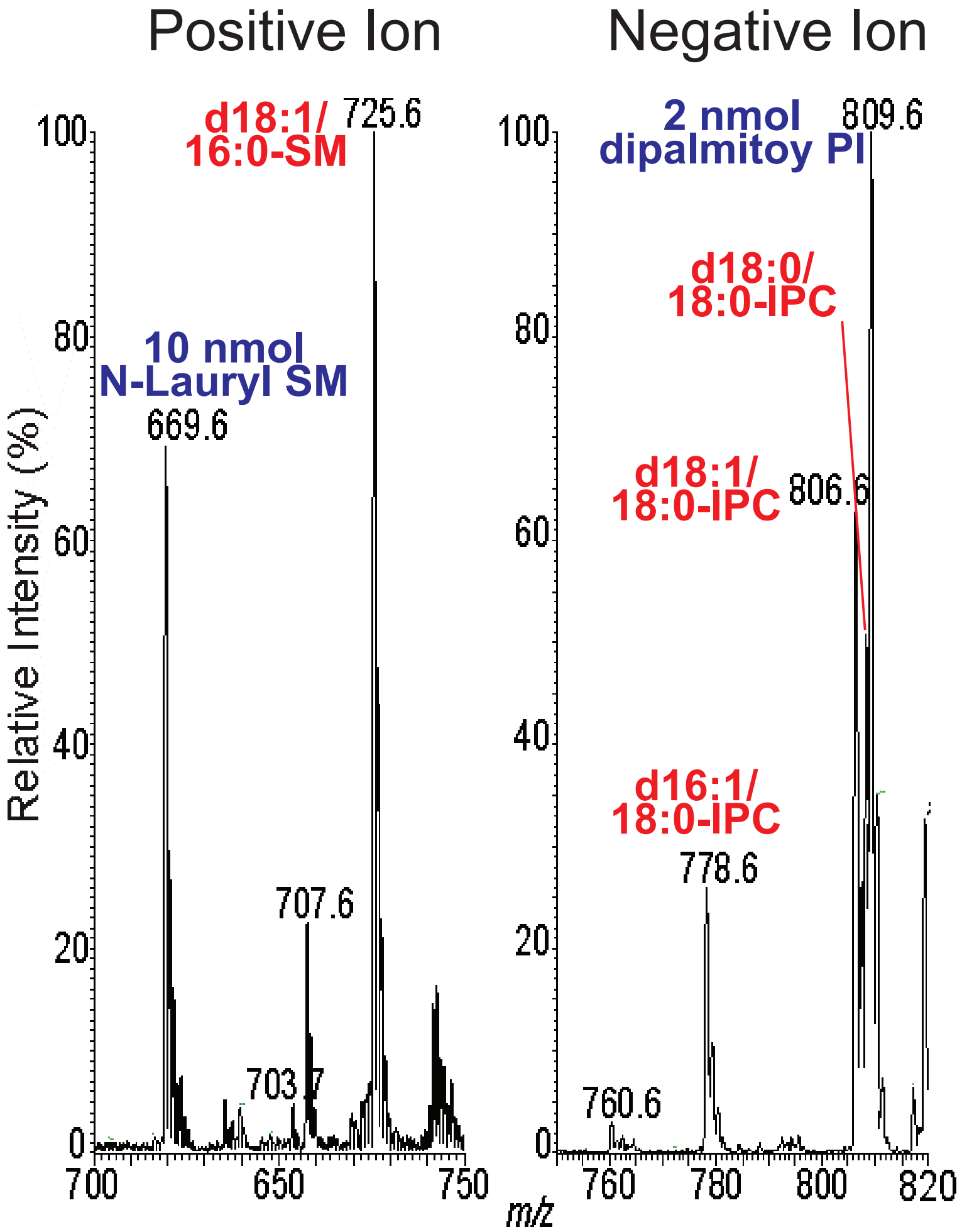
Positive Ion
Negative Ion
d18:1/
16:0-SM
725.6
10 nmol
N-Lauryl SM
669.6
707.6
703.7
2 nmol
dipalmitoy PI
809.6
d18:0/
18:0-IPC
d18:1/
18:0-IPC
806.6
d16:1/
18:0-IPC
778.6
760.6
Relative Intensity (%)
m/z
100
80
60
40
20
0
700
650
750
760
780
800
820

MS^3 (778 → 598)

A. ESI/MS protocol

(MS1) IPC m/z 778

(MS2) 598 m/z (both stages)

(MS3) Amastigotes		Promastigotes
m/z **342**	(SB derived)	**314**
360		**332**
255	(FA derived)	**283**
d18:1/16:0 IPC		**d16:1/18:0 IPC**

B. amastigote

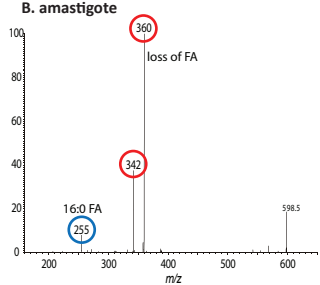

C. promastigote

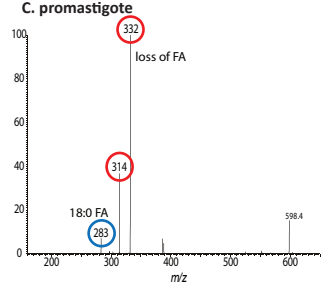

MS^3 (806 → 626)

(MS1) IPC m/z 806

(MS2) 626 m/z (both stages)

(MS3) Amastigotes		Promastigotes
m/z **342**	(SB derived)	**342**
360		**360**
283	(FA derived)	**283**
d18:1/18:0 IPC		**d18:1/18:0 IPC**

D. amastigote

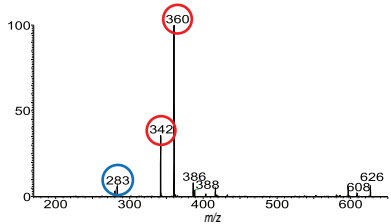

Promastigotes previously characterized in Zhang et al, 2003

MS^3 (808 → 628)

(MS1) IPC m/z 808

(MS2) 628 m/z (amastigote only)

X

(MS3) Amastigotes

m/z **344**	(SB derived)
362	
283	(FA derived)

d18:0/18:0 IPC

E. amastigote

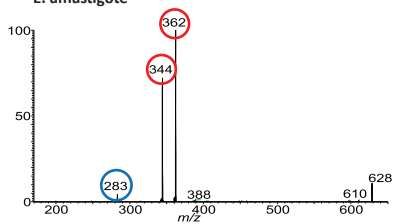

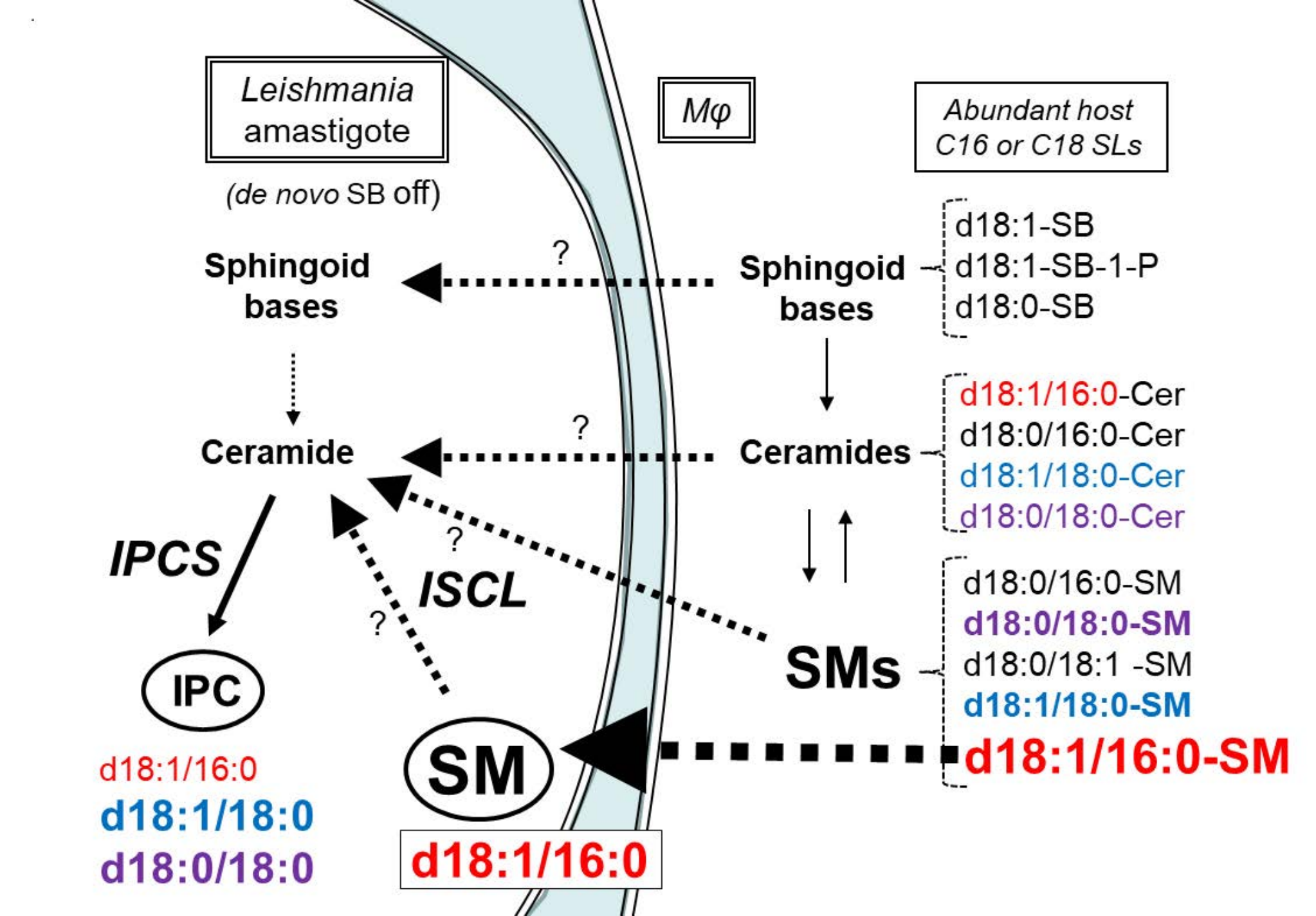
Leishmania amastigote
(de novo SB off)
Mφ
Abundant host C16 or C18 SLs
Sphingoid bases
?
Sphingoid bases
d18:1-SB
d18:1-SB-1-P
d18:0-SB
Ceramide
?
Ceramides
d18:1/16:0-Cer
d18:0/16:0-Cer
d18:1/18:0-Cer
d18:0/18:0-Cer
IPCS
?
ISCL
?
SMs
d18:0/16:0-SM
d18:0/18:0-SM
d18:0/18:1 -SM
d18:1/18:0-SM
d18:1/16:0-SM
IPC
d18:1/16:0
d18:1/18:0
d18:0/18:0
SM
d18:1/16:0

Figure S5. Total spectra, negative ion mode

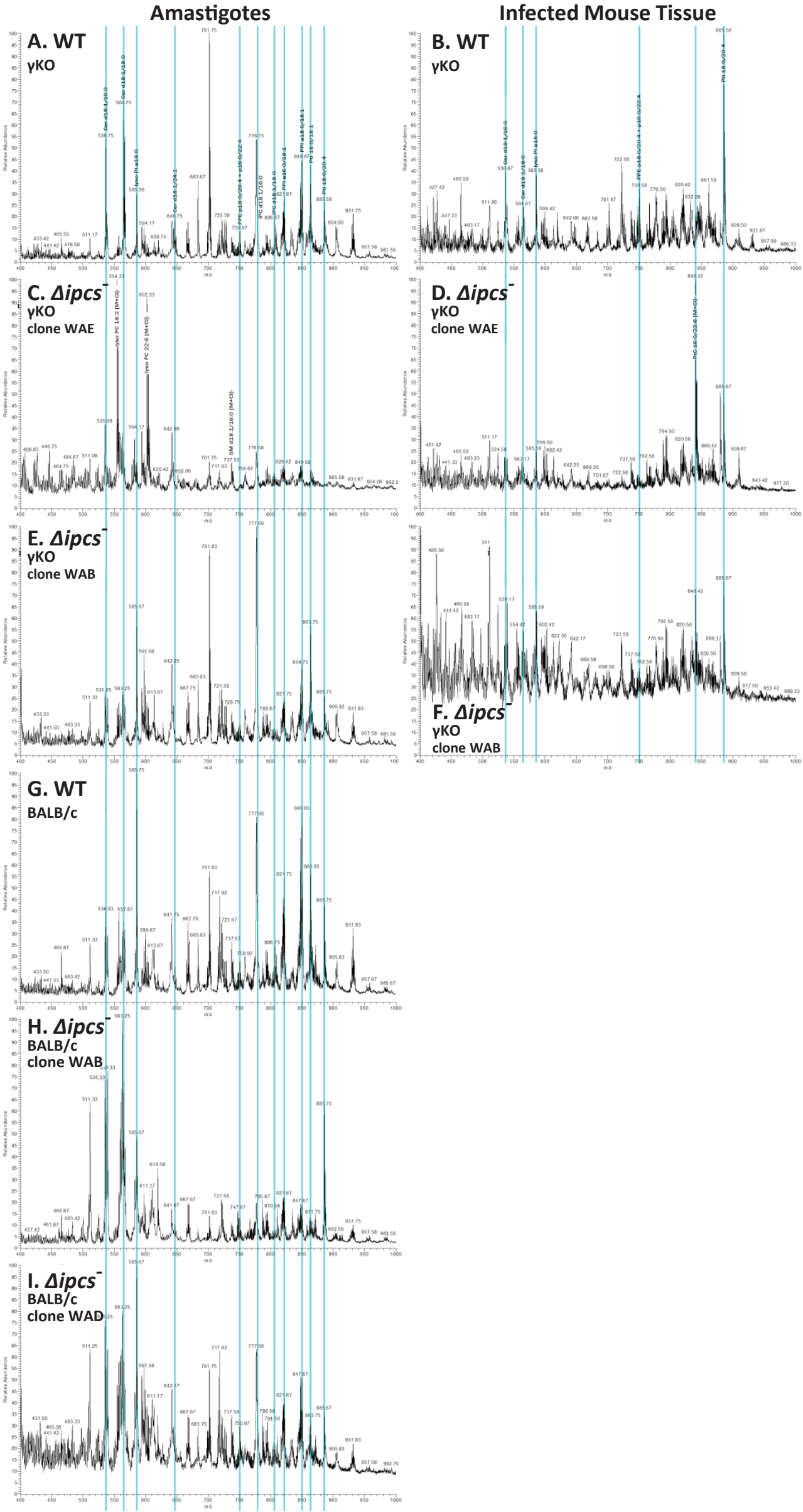

Figure S6. Total spectra, -241 negative precursor scan

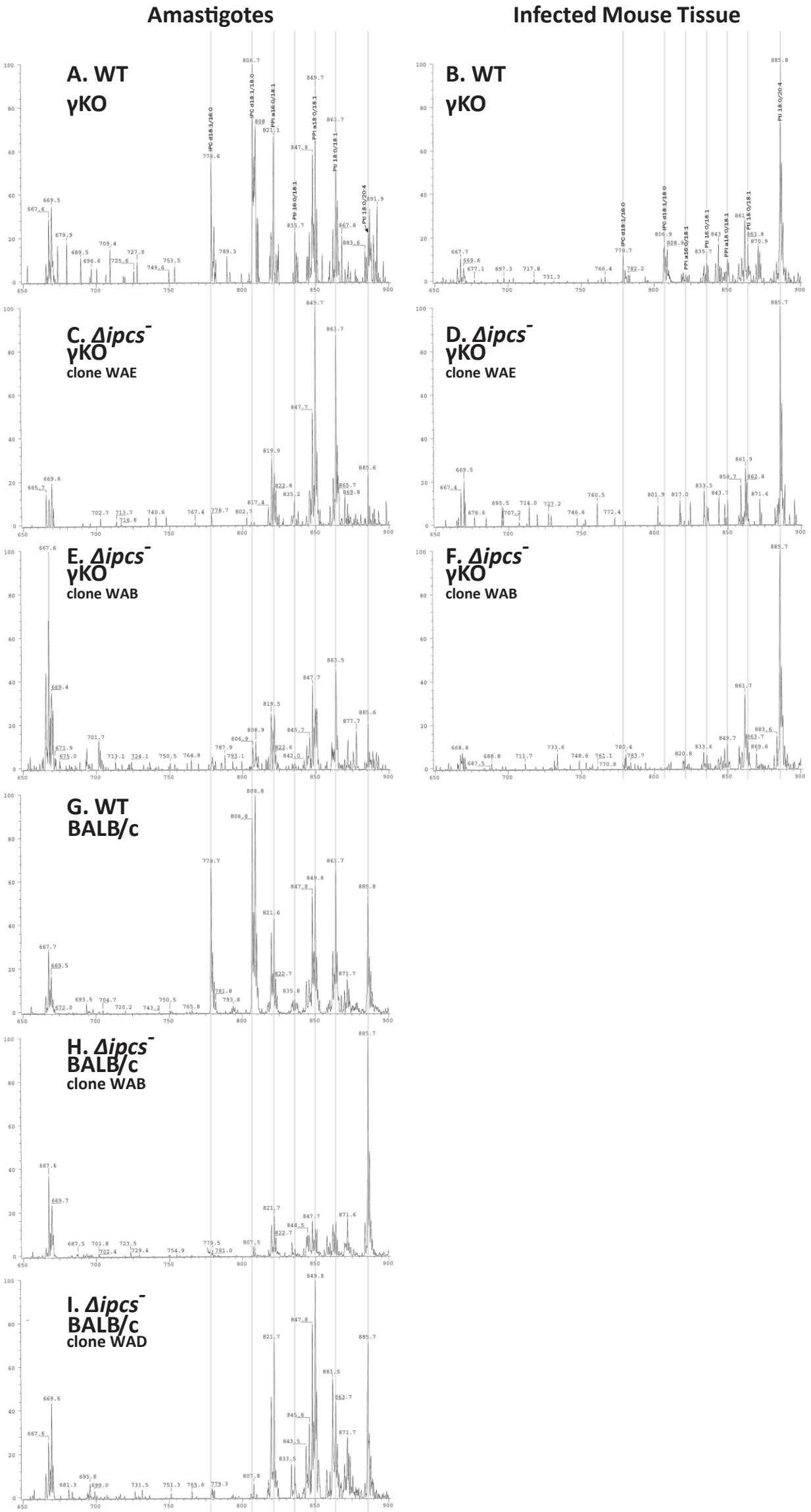
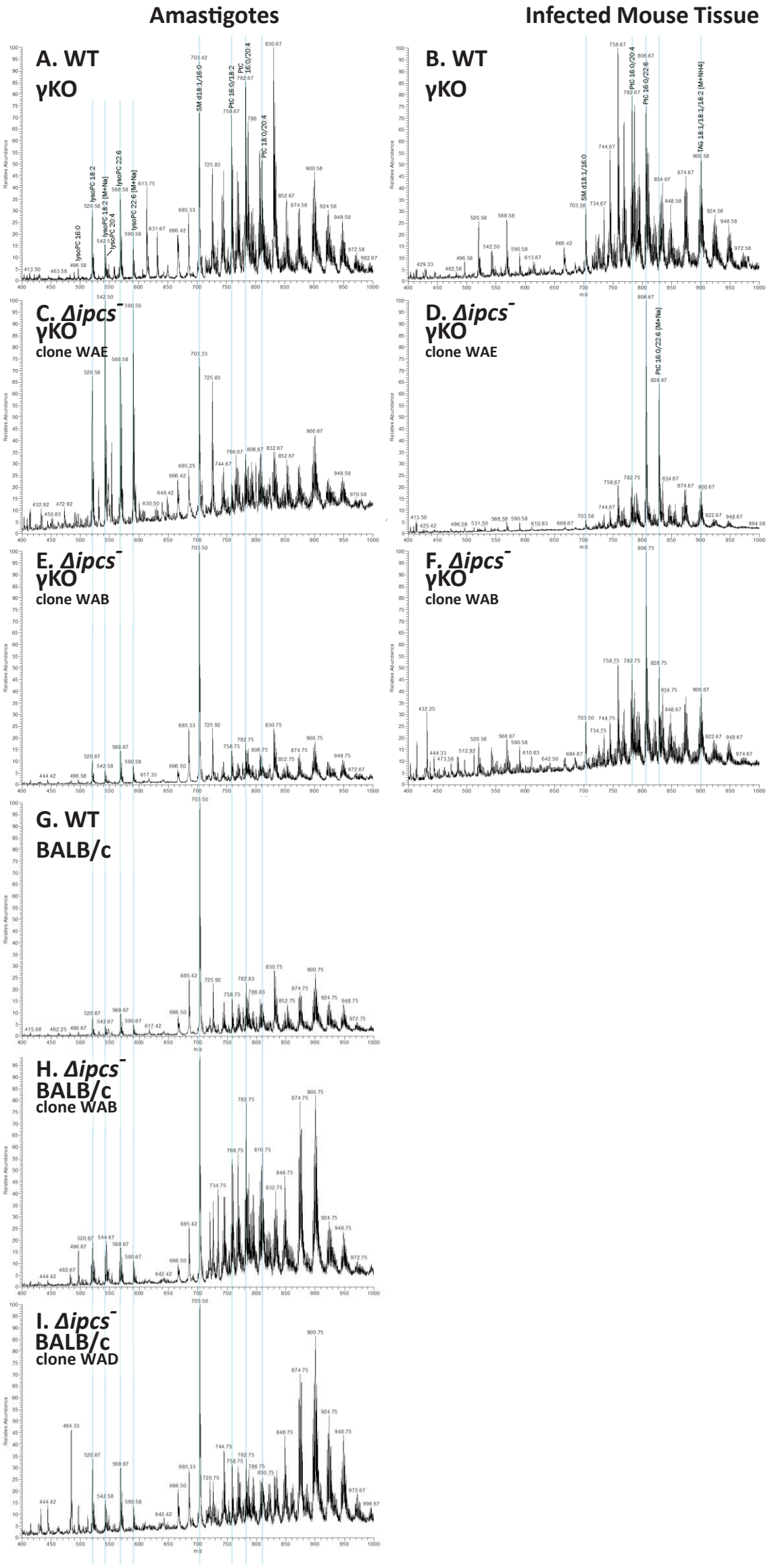
Figure S7. Total spectra, positive ion scan